





Research Article

Capturing tumour heterogeneity in pre- and post-chemotherapy colorectal cancer ascites-derived cells using single-cell RNA-sequencing

 Tiraput Poonpanichakul^{1,2,3},  Meng-Shin Shiao⁴, Natnicha Jiravejchakul²,  Ponpan Matangkasombut^{2,3}, Ekaphop Sirachainan^{5,6},  Varodom Charoensawan^{3,7,8} and  Natini Jinawath^{6,8,9}

¹Chakri Naruebodindra Medical Institute, Faculty of Medicine Ramathibodi Hospital, Mahidol University, Samut Prakan, Thailand; ²Department of Microbiology, Faculty of Science, Mahidol University, Bangkok, Thailand; ³Systems Biology of Diseases Research Unit (SyBiD), Faculty of Science, Mahidol University, Bangkok, Thailand; ⁴Research Center, Faculty of Medicine Ramathibodi Hospital, Mahidol University, Bangkok, Thailand; ⁵Division of Medical Oncology, Department of Internal Medicine, Faculty of Medicine Ramathibodi Hospital, Mahidol University, Bangkok, Thailand; ⁶Ramathibodi Comprehensive Cancer Center, Faculty of Medicine Ramathibodi Hospital, Mahidol University, Bangkok, Thailand; ⁷Department of Biochemistry, Faculty of Science, Mahidol University, Bangkok, Thailand; ⁸Integrative Computational BioScience (ICBS) Center, Mahidol University, Nakhon Pathom, Thailand; ⁹Program in Translational Medicine, Faculty of Medicine Ramathibodi Hospital, Mahidol University, Bangkok, Thailand

Correspondence: Varodom Charoensawan (varodom.cha@mahidol.ac.th) or Natini Jinawath (natini.jin@mahidol.ac.th, jnatini@hotmail.com)



Malignant ascites is an abnormal accumulation of fluid within the peritoneal cavity, caused by metastasis of several types of cancers, including colorectal cancer (CRC). Cancer cells in ascites reflect poor prognosis and serve as a good specimen to study tumour heterogeneity, as they represent a collection of multiple metastatic sites in the peritoneum. In the present study, we have employed single-cell RNA-sequencing (scRNA-seq) to explore and characterise ascites-derived cells from a CRC patient. The samples were prepared using mechanical and enzymatic dissociations, and obtained before and after a chemotherapy treatment. Unbiased clustering of 19,653 cells from four samples reveals 14 subclusters with unique transcriptomic patterns in four major cell types: epithelial cells, myeloid cells, fibroblasts, and lymphocytes. Interestingly, the percentages of cells recovered from different cell types appeared to be influenced by the preparation protocols, with more than 90% reduction in the number of myeloid cells recovered by enzymatic preparation. Analysis of epithelial cell subpopulations unveiled only three out of eleven subpopulations with clear contraction after the treatment, suggesting that the majority of the heterogeneous ascites-derived cells were resistant to the treatment, potentially reflecting the poor treatment outcome observed in the patient. Overall, our study showcases highly heterogeneous cancer subpopulations at single-cell resolution, which respond differently to a particular chemotherapy treatment. All in all, this work highlights the potential benefit of single-cell analyses in planning appropriate treatments and real-time monitoring of therapeutic response in cancer patients through routinely discarded ascites samples.

Received: 03 September 2021
Revised: 16 October 2021
Accepted: 22 October 2021

Accepted Manuscript online:
28 October 2021
Version of Record published:
07 December 2021

Introduction

Colorectal cancer (CRC) is one of the most common cancers globally. CRC exhibits high mortality rate [1] and high risk of metastasis [2]; it can progress and metastasise to several body sites, including the peritoneum. Approximately 7–26% of the CRC patients had peritoneal metastasis, resulting in malignant ascites, and this poses a poorer prognosis and higher risk of recurrence [3]. Metastasis and chemoresistance in cancer are often correlated [4,5]. However, it is challenging to accurately assess how the cancer

cells respond to chemotherapy treatments and thus determine an appropriate regimen [6]. When the direct assessment of primary tumour cells is not practical, most clinical investigations rely on known blood markers to evaluate cancer status [7–9]. Alternatively, malignant ascites, which represents another biofluid source for liquid biopsy, can serve as an important biological material for molecular characterisation of solid tumours. It is readily available in large volume when cancer patients undergo intermittent abdominal paracentesis to relieve abdominal discomfort, which is part of symptomatic treatment. However, so far there are only a few studies that characterise the potential use of malignant ascites. Some of those studies aim to find biomarkers for cancer diagnosis [10,11] or study the molecular phenotype of ascites-derived cells [12]. Furthermore, ascites is gaining recognition as a unique form of tumour microenvironment responsible for cancer progression and treatment resistance. Since there are multiple cell types in malignant ascites including tumour cells, stromal cells and immune cells [13], the ability to simultaneously analyse each cellular population and subpopulation should help clarify the roles of ascites samples in cancer progression and its potential usage as a liquid biopsy specimen.

In the era of high-throughput molecular technologies such as massively parallel sequencing, transcriptomics has been intensively applied to study the gene expression characteristics of different types of cancers. One of the most comprehensive examples of high-throughput gene expression profiling of cancers is The Cancer Genome Atlas (TCGA) project (<https://www.cancer.gov/tcga>) and Consensus Molecular Subtype (CMS) classification systems [14]. Both demonstrate the benefits of harnessing the gene expression signatures and clinical features to classify patients based on treatment responses and the disease outcomes. However, overall progress is still largely hindered by the limitations of resolving intratumoural heterogeneity, and hence the majority of the expression profiles represent the ‘average’ molecular characteristics of highly heterogeneous cancer cells [15,16].

Single-cell RNA-sequencing (scRNA-seq) is a powerful tool that enables transcriptomic profiling of individual cancer cells, and empowers clinical implementation of more tailored treatments [17–19]. It has been proposed that characterisation of transcriptomic profiles of the CRC samples using scRNA-seq would be an important step to understand the carcinogenesis and progression mechanisms of this cancer [20,21], as well as to develop personalised treatment against it [17]. In the past 5 years, several studies have employed scRNA-seq to investigate the genomic heterogeneity of CRC in several aspects. Li and co-workers, for instance, investigated the intratumoural heterogeneity of CRC cells at primary site, as compared with adjacent normal mucosal tissues [22]. Dai and co-workers investigated the heterogeneity of CRC tissue at primary site [23]. Despite being a practical source of patient samples for biomolecular analysis, to the best of our knowledge, no study so far has described intratumoural heterogeneity of malignant ascites in CRC patients. Indeed, the promising prospect of using ascites-derived cells to investigate the cancer’s molecular profile was demonstrated by Tang-Huau and co-workers, who successfully utilised scRNA-seq to dissect cellular heterogeneity and myeloid cells cross-presentation in ovarian cancer [24].

Here, we characterised intratumoural heterogeneity from ascites-derived cancer cells using a droplet-based scRNA-seq method. To investigate whether different single cell dissociation methods may alter cell population size and gene expression, the samples were prepared using different cell preparation protocols: mechanistic or enzymatic dissociation. We observed intratumoural heterogeneity and population dynamic changes between a cycle of modified FOLFIRI (mFOLFIRI) chemotherapy regimen, which corresponded well to the clinical outcome observed in our patient. Taken together, we have provided evidence of how the single-cell technology can be employed to dissect molecular complexity of intratumoural heterogeneity, the key insight required to improve the accuracy of molecular markers and the efficacy of the treatments against cancers.

Materials and methods

Patient information and clinical diagnosis

A 62-year-old female patient with underlying hypertension presented with weight loss, constipation, and haematochezia. CT colonoscopy showed polypoid polyps at distal rectum. Sigmoidoscopy showed 50% circumferential mass at 5–15 cm from anal verge with partial obstruction. Pathology report of the biopsy sample showed moderately differentiated adenocarcinoma. Molecular study of the tumour showed KRAS codon 12 (G12C) mutation. CT scan of whole abdomen revealed two small (7 and 8 mm) hypodense lesions at hepatic segments VII and VIII, circumferential irregular enhancing wall of rectum 5.6 cm from anal verge, perirectal fat extension, and multiple perirectal lymphadenopathy. Chest CT scan showed multiple lung nodules (2–4 mm). The patient was diagnosed with advanced rectal cancer (cT3N2bM1) with lung and liver metastases.

Clinical course and treatment history

A palliative chemotherapy, modified FOLFOX6 (mFOLFOX6), was started in November 2017. After the fourth cycle, MRI showed a decrease in size of liver nodule in segment VIII from 8 to 4 mm, and disappearance of segment VII nodule. The patient received two more cycles of mFOLFOX6, then requested to change the regimen due to intolerable side effects, and thus was switched to capecitabine/oxaliplatin (CapeOx). Due to thrombocytopenia and neuropathy, oxaliplatin dose was reduced and finally omitted. After the fourth cycle of CapeOx, she developed abdominal distension from massive ascites. CT scan showed peritoneal metastasis but rectal mass size was decreased and no liver nodule was found. Progressive disease was diagnosed. She underwent abdominal paracentesis. The ascites cytology showed adenocarcinoma. She then received a second-line palliative chemotherapy, mFOLFIRI, in May 2018. Ascitic fluid samples were collected before and after the first cycle of mFOLFIRI. Carcinoembryonic antigen (CEA) slightly changed from 6.8 to 6.4 ng/ml after the treatment. Later, the patient developed new pleural effusion after the second cycle of mFOLFIRI and required frequent thoracocentesis and abdominal paracentesis procedures. Bevacizumab was added to mFOLFIRI in the third cycle in July 2018. Finally, her performance status declined gradually, she could not receive any further palliative chemotherapy and best supportive care was given. All samples were obtained with informed consent after the approval from the Institutional Review Board at Faculty of Medicine Ramathibodi Hospital, Mahidol University under certificate number COA.MURA2018/1067. Detailed clinical timeline can be found in Supplementary Figure S1.

Patient sample collection and single cell preparation

Approximately 500 ml of ascitic fluid was collected from the patient and was transferred to the laboratory for processing immediately. Ascites was pre-filtered by 70- μ m cell strainers (Corning, cat. no. 431751, U.S.A.) with gentle mechanical motorisation using pipette tips to assist cell clumps to pass through filters. The filtered ascitic fluid was collected in 50-ml falcon tubes. Cells in the filtered ascites were then subjected to centrifugation at 100 rcf for 10 min at 25°C and the clear supernatant was carefully removed. Next, the sedimented cells were treated with the RBC lysis buffer (Qiagen, cat. no.158902, Germany) to remove the red blood cells (RBCs). One millilitre of pre-chilled RBC lysis buffer was gently mixed with the cells, and incubated at room temperature for 5–10 min depending on the observed amount of RBCs in the cell pellets. Ten millilitres of pre-chilled Dulbecco's phosphate-buffered saline (DPBS, calcium- and magnesium-free) was later added and cells were again collected by centrifugation at 300 rcf for 10 min at 25°C. For mechanical dissociation, the cells were assessed again under the microscope; if many cell clumps were still visualised, another round of filtering with 70- μ m cell strainers was applied. For enzymatic dissociation, after RBC removal, we treated the cells with 2 ml of Accumax (Innovative Cell Technologies, Inc., U.S.A.) and incubated the cells at 37°C for 10 min, after which the cells were quickly assessed under the microscope. If there were still many visible cell clumps, another 10–20-min incubation was applied. Accumax reaction was terminated by the addition of 10-ml fresh culture medium, followed by centrifugation at 300 rcf for 10 min at 25°C to collect cell pellets. Finally, viable cell numbers after the completion of both dissociation methods were assessed by haemocytometer using Trypan Blue. The single cells were then resuspended in 90% FBS+10% DMSO at a concentration of 10^7 cells/ml per tube, kept in a slow-cooling freezing container at -80°C , and cryopreserved in the vapour phase of liquid nitrogen the next day for long-term storage.

scRNA-seq library preparation

Frozen cells were thawed and processed according to the recommended protocol for human PBMCs (10x Genomics, U.S.A.). Cell quantity and viability were checked with the haemocytometer under the microscope. Dead Cell Removal Kit (Miltenyi Biotec, cat. no. 130-090-101, Germany) was applied according to the manufacturer's protocol. Cells were resuspended in phosphate-buffered saline (PBS) supplemented with 0.04% bovine serum albumin (BSA) (Merck, cat. no. 12659, Germany) before undergoing single-cell preparation protocol using the Chromium Single Cell 3' v2 (10x Genomics, cat. no. PN-120267, U.S.A.). scRNA-seq libraries were sequenced with the Illumina HiSeq platform by Macrogen Inc. (South Korea).

Bioinformatics analyses

Sequenced reads were checked for overall sequencing qualities using FastQC [25], and then mapped, and unique molecular identifiers (UMIs) quantified using Cell Ranger version 3.0.1 (10x Genomics, U.S.A.), using 10x human genome GRCh38 version 1.2.0 as the reference. Seurat [26] package v3.1.0 was mainly used for further analysis, including discarding low-quality cells in the case that the number of expressed genes is less than 200 genes per cell, or the percentage of mitochondrial genes is higher than 20% in a cell. Genes that were detected in less than five cells

were also removed. SoupX [27] was applied to regress out the ambient RNAs. Doublets were determined using DoubletFinder [28], and removed from further downstream analysis. Dimensionality reduction, principal component analysis (PCA), with the top 2000 highly variable genes (default settings) as input, was performed on each library individually. The results were then normalised with *sctransform* [29] using 30 principal components (PCs). The data from different samples were then integrated using Seurat [26] package v3.1.0. Uniform Manifold Approximation and Projection (UMAP) [30] was used for data visualisation. Populations of cells with similar transcriptomic profiles were clustered using the Leiden algorithm [31]. A total of 14 clusters were identified (Supplementary Figure S2), and annotated according to known marker genes for epithelial cells (*EPCAM*, *KRT18*), fibroblasts (*SPARC*, *COL3A1*), myeloid cells (*CD14*, *S100A8*, *CD68*), and lymphocytes (*PTPRC*, *CD3D*, *CD79A*). Differentially expressed genes (DEGs) were determined using Wilcoxon's rank sum test with Bonferroni correction for multiple tests. ComplexHeatmap was used to generate heatmaps for gene expression visualisation [32]. The epithelial cells were further extracted, re-normalised, and re-integrated. Cell clustering and dimensionality reduction were performed as described above. Gene set enrichment analysis (GSEA) [33] was done using the *fgsea* package [34] with default parameters. Input for GSEA was ranked by average log2 fold change derived from the *findmarker* function, comparing each cluster and other cells with parameter *logfc.threshold* = 0, *min.pct* = 0, and *min.diff* = $-\text{Inf}$, in order to keep all genes as the input. Hallmark gene sets were used to assess biological process and state of gene expression [35]. In addition, publicly available data of normal gastrointestinal tract obtained from GSE125970 [36], were re-processed using the same pipeline as described above, and integrated with the single-cell data from this study.

Results

Collection of ascites from a CRC patient and cell preparation

Ascites-derived cells were collected from a CRC patient and processed as described in 'Materials & methods' section. Briefly, a 62-year-old woman had been diagnosed with advanced CRC (cT3N2bM1) with lung and liver metastases, and was under a course of first-line chemotherapy. However, the patient condition worsened due to intolerable side effects and she developed malignant ascites. Treatment regimen was then changed to mFOLFIRI. To investigate the treatment responsiveness of metastasised cancer cells, the ascites fluid samples, which were tapped and collected twice, before and after the first cycle of mFOLFIRI, were subjected to scRNA-seq profilings (see complete treatment scheme in Supplementary Figure S1). The samples were prepared by enzymatic and mechanical protocols, giving rise to a total of four samples to be further processed by scRNA-seq, namely Pre-tx enzymatic, Pre-tx mechanical, Post-tx enzymatic, and Post-tx mechanical. Accumax was selected as the enzyme of choice because it is less toxic and gentler on cells than trypsin and collagenase. Single-cell isolation, RNA extraction, and reverse transcription were carried out according to the 10x Genomics manufacturer's protocols. Data analyses to elucidate the effect of different sample preparation protocols and the effect of chemotherapy on ascites cells were performed (Figure 1).

Overall scRNA-seq profiles of pre- and post-chemotherapy CRC ascites-derived cells

From the four samples, we were able to profile transcriptional patterns of the total of 19,653 cells, with the number of cells from each individual sample ranging from 3,176 to 6,809 cells (Figure 2A, Supplementary Table S1). Interestingly, our scRNA-seq profiling revealed previously unappreciated heterogeneous cell populations comprising multiple cell types across the samples. In this particular case, the most abundant cell types found in the ascites-derived populations of cells were epithelial cells (85.84%), myeloid cells (9.11%), fibroblasts (0.67%), and other smaller populations of cells (4.36%). Figure 2B demonstrates the marker genes and their expression prevalence employed to identify the main populations (see also figure legend and 'Materials and methods' section for data clustering information and cell type classification). To further verify the cell types assigned, we used the function 'FindMarker' in the Seurat toolkits [26] to unbiasedly extract the most representative set of genes uniquely expressed in different populations, namely epithelial cells (*EPCAM*, *KRT8*, *KRT18*), fibroblasts (*SPARC*, *COL3A1*, *COL1A1*), and myeloid lineage (*S100A8*, *CXCL8*, *IL1B*) (Figure 2C). For 'other' smaller populations of cells, we observed the expression of *CD3E*, *CD79A* and *NKG7*, suggesting that this group of cells might contain a mixture of T cells, B cells, and NK cells.

Choice of cell dissociation methods highly influenced scRNA-seq profiles

We next asked if and how the methods of cell dissociation and/or that particular cycle of mFOLFIRI treatment had effects on the populations of identifiable cell types, as well as their gene expression profiles. Indeed, the most apparent differences in the percentages of recovered cell populations were between the enzymatic and mechanical dissociation protocols, especially between the two pre-treatment samples (Figure 3A,B). Strikingly, we observed that a higher pro-

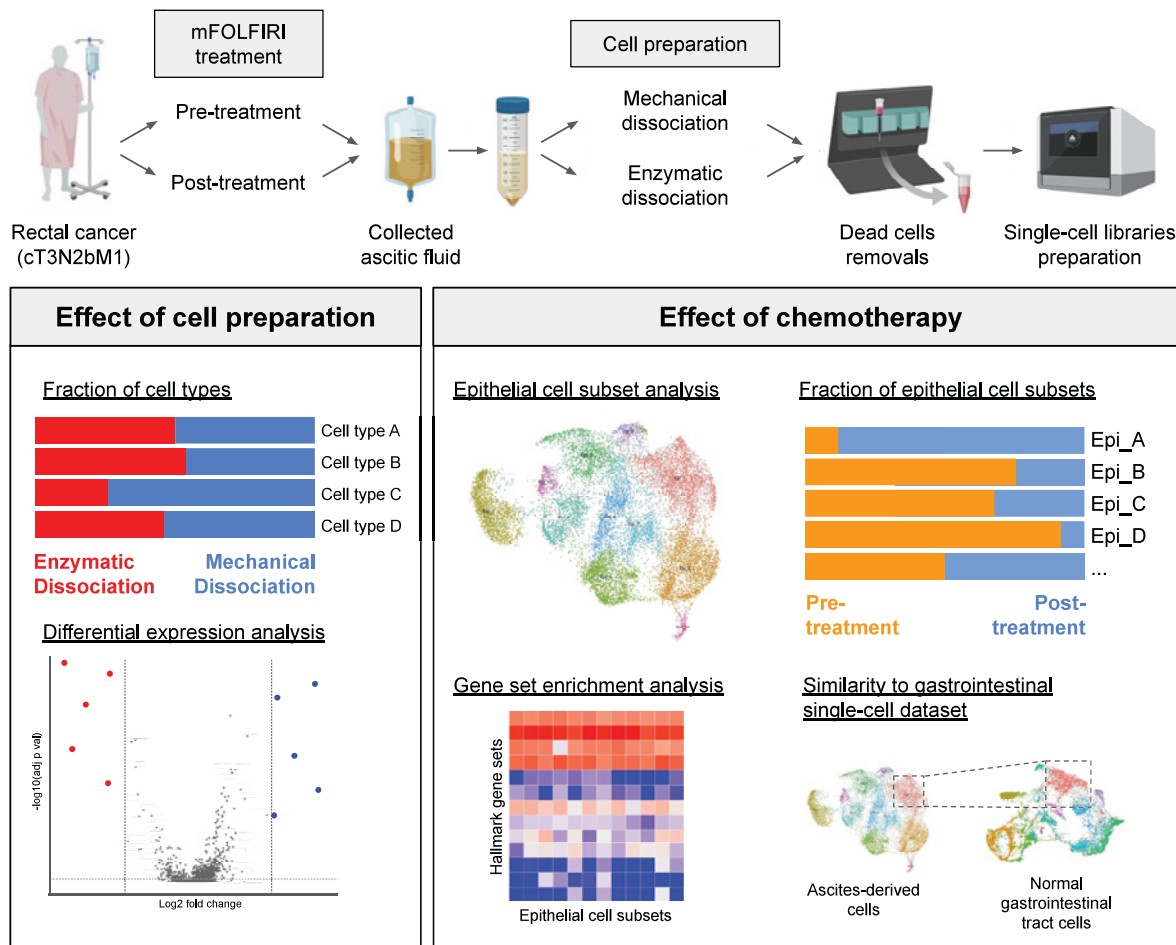


Figure 1. A summary flowchart showing the clinical course of the patient and study design

Ascitic fluids were collected before and after a course of mFOLFIRI treatment in a patient with rectal cancer. The samples collected from each time point were prepared for single-cell transcriptomic analysis using either mechanical or enzymatic dissociation methods. All the samples were subjected to quality control and removal of dead cells, and only viable single-cell suspensions were used for the scRNA-seq experiment on the 10x Genomics platform (see also ‘Materials and methods’ section and Supplementary Figure S1 for more details). Subsequent data analysis explored the effect of sample preparation by comparing the fraction of captured cell types and DEGs between two preparation protocols. Further analyses investigated the effect of chemotherapy by comparing each fraction of epithelial cell subsets, GSEA, and comparing the expression profile to that of normal gastrointestinal scRNA-seq data.

portion of myeloid cells were captured using the mechanical dissociation protocol (32.2 and 2.5%; Pre- and Post-tx), as compared with that of enzymatic preparation (3.1 and 1.6%; Pre- and Post-tx). As a result, the enzymatic preparation yielded slightly higher relative proportions of epithelial cells and fibroblasts, 95.4/91.7% and 0.8/0.9% respectively, as compared with 66.2/85.4% and 0.2/0.7% from the mechanical preparation samples.

In addition to the compositions of cell types found in the ascites samples, we also sought to determine whether the dissociation methods also affected the gene expression profiles. Differential expression (DE) analysis focusing on the epithelial cells obtained using the two dissociation methods showed that *HES1*, *IER3*, *JUNB*, *IER2*, *SOCS3*, and *ID1* were detected at significantly higher levels in the enzymatically dissociated samples than those obtained from the mechanically dissociated ones (Figure 3C,D and Supplementary Table S2). In addition, several genes encoding epithelial cell surface proteins and cytoskeletons such as *CLDN4* (Claudin 4), *SFN* (Stratifin), *LMNA* (Lamin A/C), *KRT17* (Keratin 17), and *EMP1* (Epithelial Membrane Protein 1) were also found at higher levels in the enzymatically dissociated samples. On the contrary, we found that *CD81* (Tetraspanin) and *PPP1CB* (Protein Phosphatase 1 Catalytic Subunit β) were under-represented in the enzymatically prepared samples. DE analyses of the myeloid

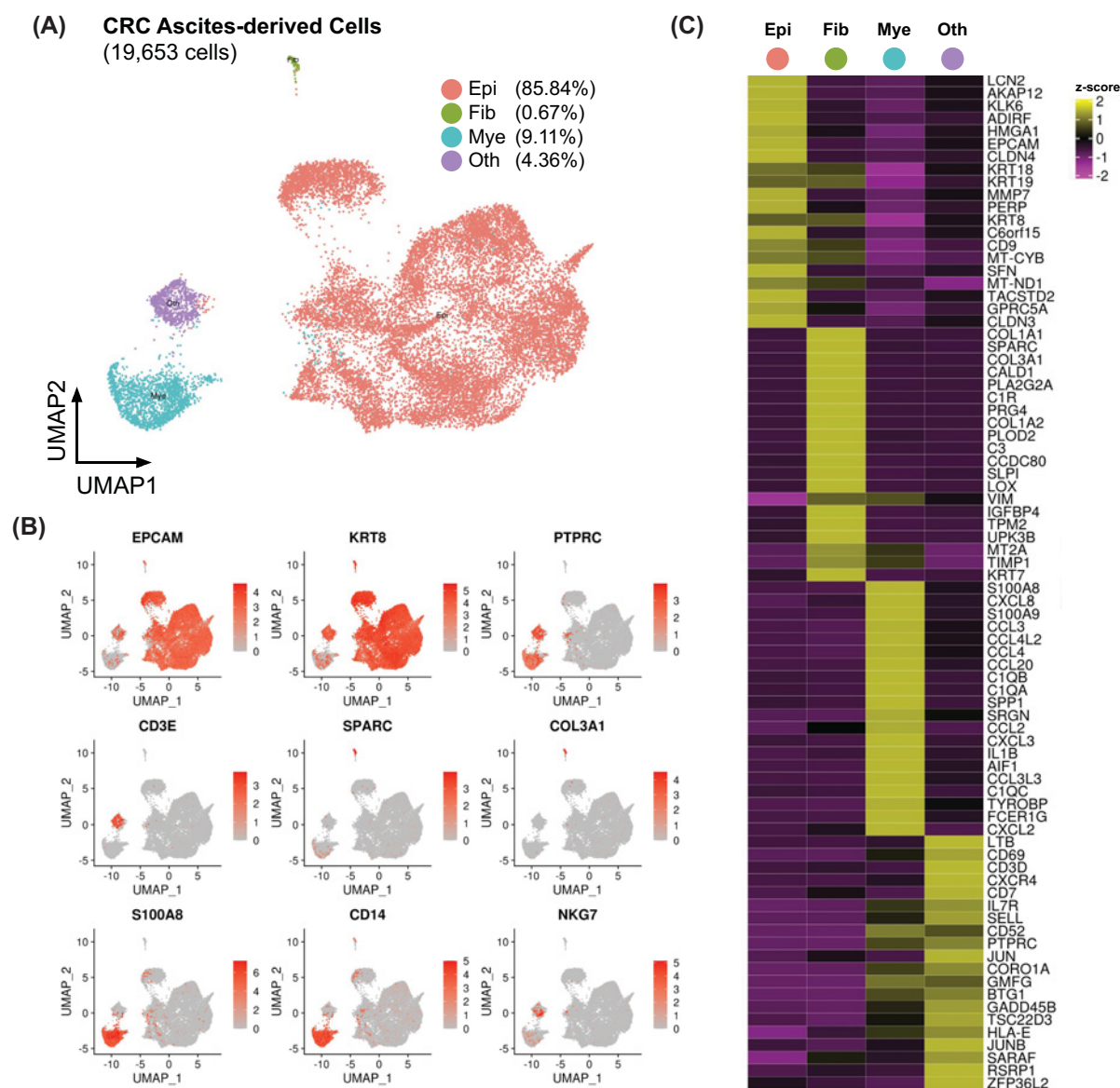


Figure 2. Profiling the pre- and post-chemotherapy CRC ascites-derived cells with scRNA-seq reveal heterogeneous cell populations across the samples

(A) UMAP dimensional reduction plot of integrated data (four samples) overlaid with major cell type annotations. Epithelial cells accounted for the majority of the cells in the ascitic fluids from the patients. (B) UMAP dimensional reduction plot overlaid with normalised gene expression values of known marker genes of epithelial cells (*EPCAM*, *KRT8*), fibroblasts (*SPARC*, *COL3A1*), myeloid cells (*S100A8*, *CD14*), and other mixed lymphocytes (*PTPRC*, *CD3E*, *NKG7*). (C) Heatmap showing top ten marker genes for each of the major cell type (Epi, epithelial cells; Fib, fibroblasts; Mye, myeloid cells; Oth, other cells), as determined unbiasedly using *Seurat findmarker* function [26]. Yellow indicates relative overexpression as compared with other cell types, whereas purple indicates relative down-regulation.

cells showed that several chemokines and cytokine genes, such as *CCL3*, *CCL4*, *CXCL8*, *IL6*, and *IL1B* were found at low levels in the samples prepared by the enzymatic dissociation, in accordance with low percentages of myeloid cell population (Supplementary Figure S3). These results further demonstrate the effects of enzymatic and mechanical dissociations on not just the relative abundance of cell populations, but also on the gene expression profiles.

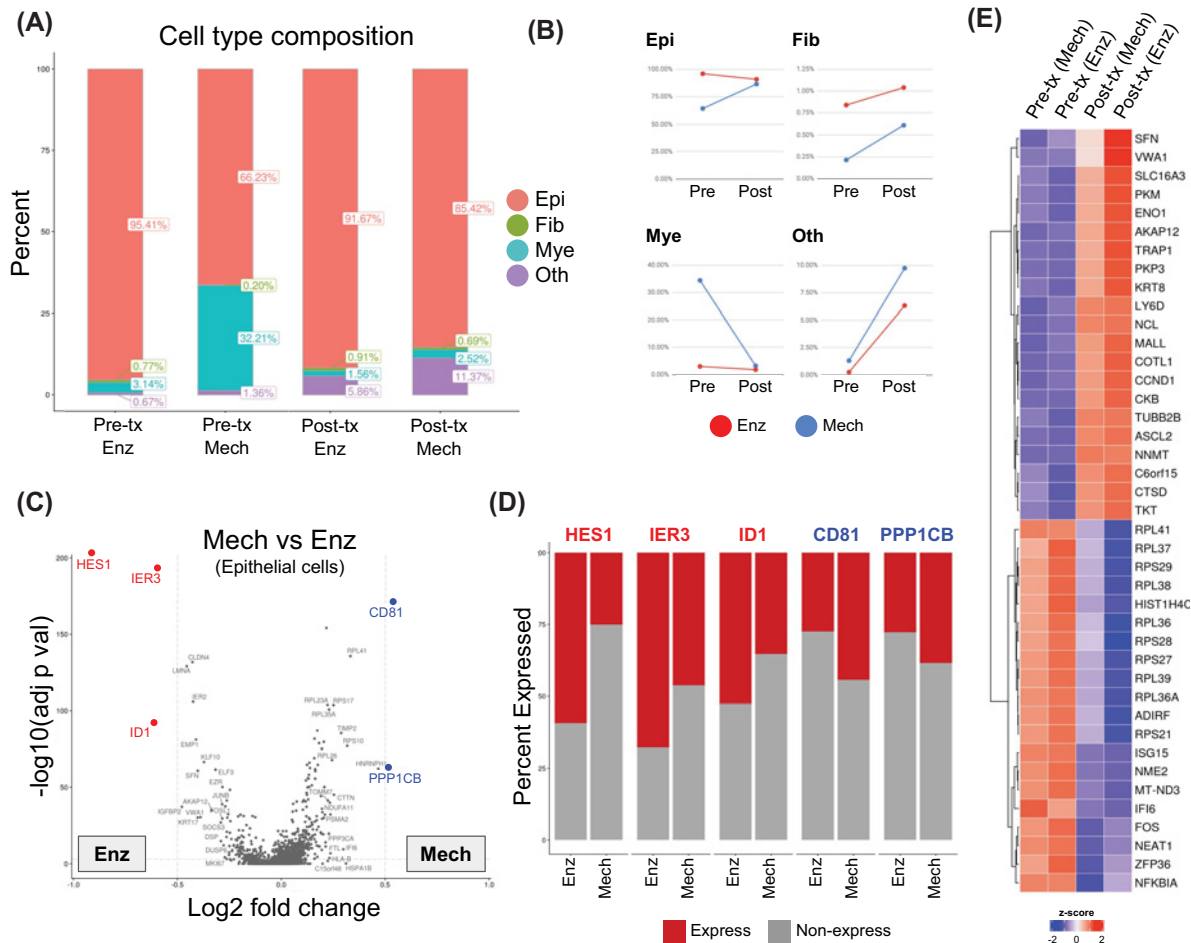


Figure 3. The effect of single-cell preparation methods (mechanical versus enzymatic dissociation) on gene expression
(A) Bar graphs showing the fractions of the four major annotated cell types (Epi, epithelial cells; Fib, fibroblasts; Mye, myeloid cells; Oth, other cells) found in each sample and condition (Pre-tx, pre-treatment; Post-tx, post-treatment; Enz, enzymatic dissociation; Mech, mechanical dissociation). (B) Line plots showing the effects of sampling time point and preparation protocol on the frequency of each of the four major cell types. Dots and lines connect the pre- and post-treatment samples with the same preparation methods to show the trends between the two time points. (C) Volcano plots showing DEGs from the comparison between mechanical and enzymatic preparations of the epithelial cells, red and blue represent the up-regulated genes appeared in the enzymatic preparation as compared with mechanical preparation, and *vice versa* respectively. Coloured dots highlighted genes that have log2 fold change > 0.5 and adjusted *P*-value < 0.01. (D) Bar plots showing a fraction of cells expressing DEGs from (C). Expressed fraction is determined by the number of cells having expression level more than quartile 1 (25%) of all the cells expressing that particular gene. (E) Heatmap showing DEGs from the comparison between the post- and pre-treatment epithelial cells. Red indicates relative overexpression as compared with other conditions, whereas blue indicates relative down-regulation.

Effect of the chemotherapy regimen, mFOLFIRI, on cellular heterogeneity and gene expression of ascitic cells

We observed that the proportions of the cells assigned to the epithelial cluster were largely unchanged before and after the treatment, as compared with the effect from the dissociation methods. Looking in more detail; however, the relative fractions of myeloid cells appeared to shrink slightly; whereas those of fibroblasts and the 'others' showed slightly increasing numbers in the samples from both dissociation methods (Figure 3A,B). We noted that, due to the limitation of the number of samples analysed here, these trends should be regarded as observations rather than confirmation, and thus would require further validation in additional patients.

Next, we sought to get an overview of transcriptomic profile changes of the epithelial cancer cells found in the ascites samples, before and after the mFOLFIRI treatment, by comparing the gene expression of epithelial cells as a whole, also known as 'pseudo-bulk' RNA-seq. DEGs are visualised using a heatmap (Figure 3E). After looking at genes that pass the selection threshold (\log_2 fold change > 0.5 and adjusted P -value < 0.001), several ribosomal proteins encoded genes (e.g., *RPL36*, *RPL36A*, *RPL37*, *RPL38*, *RPL41*, *RPS21*, and *RPS29*) along with interferon-stimulated genes (*ISG15* and *IFI6*) are found to be lower expressed after the treatment. However, Gene Ontology (GO) term enrichment analyses of either up- or down-regulated genes did not result in any statistically significant gene set.

scRNA-seq revealed treatment-susceptible and -resistant subpopulations

As the pseudo-bulk analysis cannot fully demonstrate the changes of gene expression profiles of highly heterogeneous malignant ascitic cells, we therefore further analysed the epithelial cells in a greater depth by subsetting and re-clustering them based on their distinct transcriptomic profiles. In total, 11 transcriptionally distinct epithelial cell subclusters were annotated (Figure 4A,B). In the majority of the subclusters, the fractions of cells detected from different samples pre- and post-treatment, were largely comparable, except for the subclusters Epi_3, Epi_9, Epi_10, and Epi_11. The cells in Epi_3 were mainly from the post-treatment samples, regardless of the dissociation methods; whereas the cells in Epi_9, Epi_10, and Epi_11 were mainly found in the pre-treatment samples. This suggested possible differences in the degree of response to the treatment, as Epi_3 might be a relatively resistant population or clone that was able to expand after the treatment; whereas Epi_9, Epi_10, and Epi_11 might represent the clones that responded relatively well to that particular round of treatment.

As different epithelial cell subclusters possessed unique transcriptional characteristics, we next investigated the gene expression profiles of these subclusters, by obtaining the top five 'marker genes', or the most highly expressed genes in each cluster, as compared with the rest of the epithelial subclusters (Figure 4C). Among the diverse groups of marker genes identified, Epi_3 uniquely expressed a high level of genes encoding heat shock protein and proteasome (e.g., *HSP90AB1*, *PSMA4*). Epi_9's marker genes include the members of matrix metalloproteinase and tetraspanin families (e.g., *MMP3*, *TSPAN8*), whereas Epi_10's marker genes are related to DNA damage (e.g., *DDIT3*, *GADD45B*). Epi_11's marker genes include the members of the insulin-like growth factor-binding protein family, IGFBP6 and IGFBP7, both of which are expressed in vascular endothelial cells and mesenchymal stromal cells [37–39]. The complete list of representative genes from each of the 11 clusters is shown in Supplementary Table S3.

Possible biological mechanisms underlying the chemotherapy treatment susceptibility and resistance

We next investigated the putative functional profile of each subcluster based on the GSEA of the hallmark gene set collection from MSigDB [35] (Figure 5A). The signature genes of unfolded protein responses were highly represented in Epi_6, as several heat shock protein-coding genes including *HSPA6*, *HSPA1A*, and *HSPA1B*, were highly expressed in Epi_6. Whereas Epi_2, Epi_3, and Epi_4 were significantly enriched in the gene sets involved in cell cycling (mitotic spindle, G₂/M checkpoint, E2F targets, MYC targets) and metabolism (oxidative phosphorylation, fatty acid metabolism). Only Epi_3 was uniquely enriched in protein secretion and peroxisome pathways. Epi_3, Epi_4, and Epi_6 were also enriched with the MTORC1 signaling pathway. The mammalian target of rapamycin (mTOR) is known to be involved in regulation of cell survival, tumour progression, and anti-cancer drug resistance in many types of cancer, including CRC [40]. Interestingly, the subclusters that appeared to respond to mFOLFIRI treatment, Epi_9, Epi_10, and Epi_11, did not show any statistically significant enrichment of the hallmark gene sets.

To further explore potential functions and biological relevances of these epithelial cell subclusters, we also compared our ascitic-derived scRNA-seq data from the CRC patient with the publicly available normal intestine scRNA-seq profiles [34] (Figure 5B). Among all the subclusters, we found that Epi_11 showed the most closely related expression profile to the normal enteroendocrine cells, of which are determined by close proximity coordination on the UMAP plot of integrated data. Epi_11 might potentially possess the most sensitive phenotype to the treatment, and thus it was almost completely eradicated from the post-treatment samples. Epi_9's expression profile was closely related to normal enterocytes, whereas Epi_10's expression profile is closely related to progenitor cells. The Epi_2 cluster showed close proximity to transit amplifying (TA) cells. TA cells are normally divided from normal stem cells and later differentiated into enterocytes [41,42]. Presence of gene expression profile of TA cells might reflect the stemness phenotype of cancer cells. Notably, the expression profiles of Epi_3 and Epi_4 only showed minimal similarity when compared with the public dataset; therefore, they appeared to represent the cell populations that were unique in malignant ascites samples. This suggested that Epi_3 and Epi_4 might be highly mutated cancer cells that did not share gene expression profiles with those of normal intestinal cells, as the other subclusters of ascites-derived cells did.

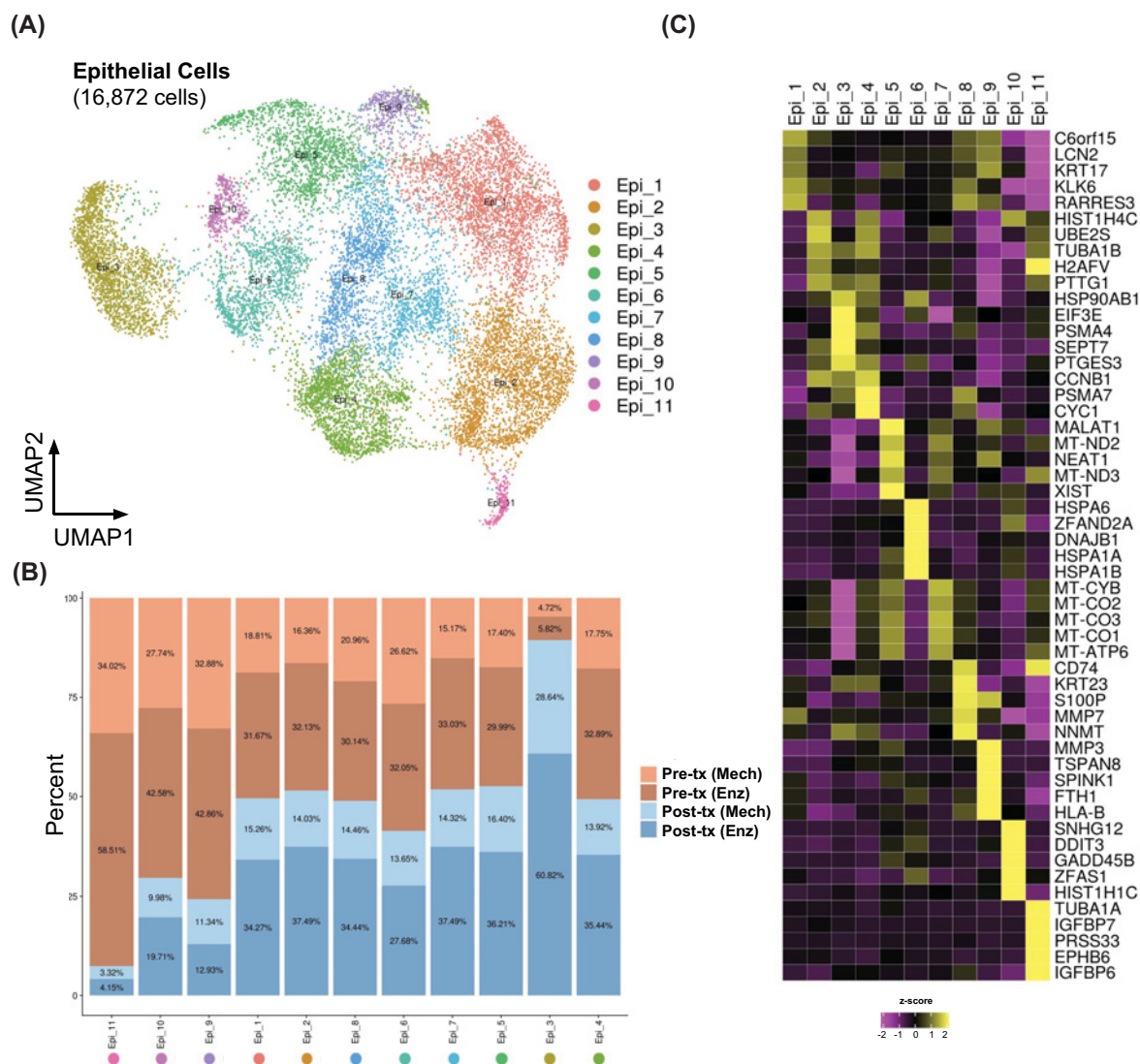


Figure 4. Epithelial cell clusters found in the CRC ascites were highly heterogeneous

(A) UMAP of reclustered epithelial cells overlaid with subcluster annotations, showing gene expression heterogeneity even within the epithelial cells. (B) Bar plots showing sample composition of each subcluster in (A). (C) Heatmap showing the top five marker genes for each subcluster. Yellow indicates relative overexpression as compared with other subclusters, whereas purple indicates relative down-regulation.

Discussion

Single-cell transcriptomics has been used extensively to investigate several biological problems, cancer biology included, in the past decade [43]. Previous studies have investigated CRC at the single-cell resolution [22,44–48], and they have demonstrated the intratumoural heterogeneity and lineage development. In the present study, we have comprehensively investigated a case of advanced CRC using the ascites-derived cells, which can serve as a practical proxy for disease monitoring as it can be routinely collected from the patients undergoing abdominal paracentesis as part of the treatment. Through the gene expression analysis at single-cell resolution, we have showcased the intratumoural heterogeneity of cancer cells, the influence from cell preparation methods, and the changes of the cancer subpopulation landscape after a cycle of chemotherapy.

Ascites-derived cells have been used to study molecular mechanisms of cancers, including ovarian and gastrointestinal cancers, particularly to investigate disease progression and treatment responsiveness [49–55]. However, identification of biomarkers can be complicated by the heterogeneous cellular compositions. Using scRNA-seq profiling

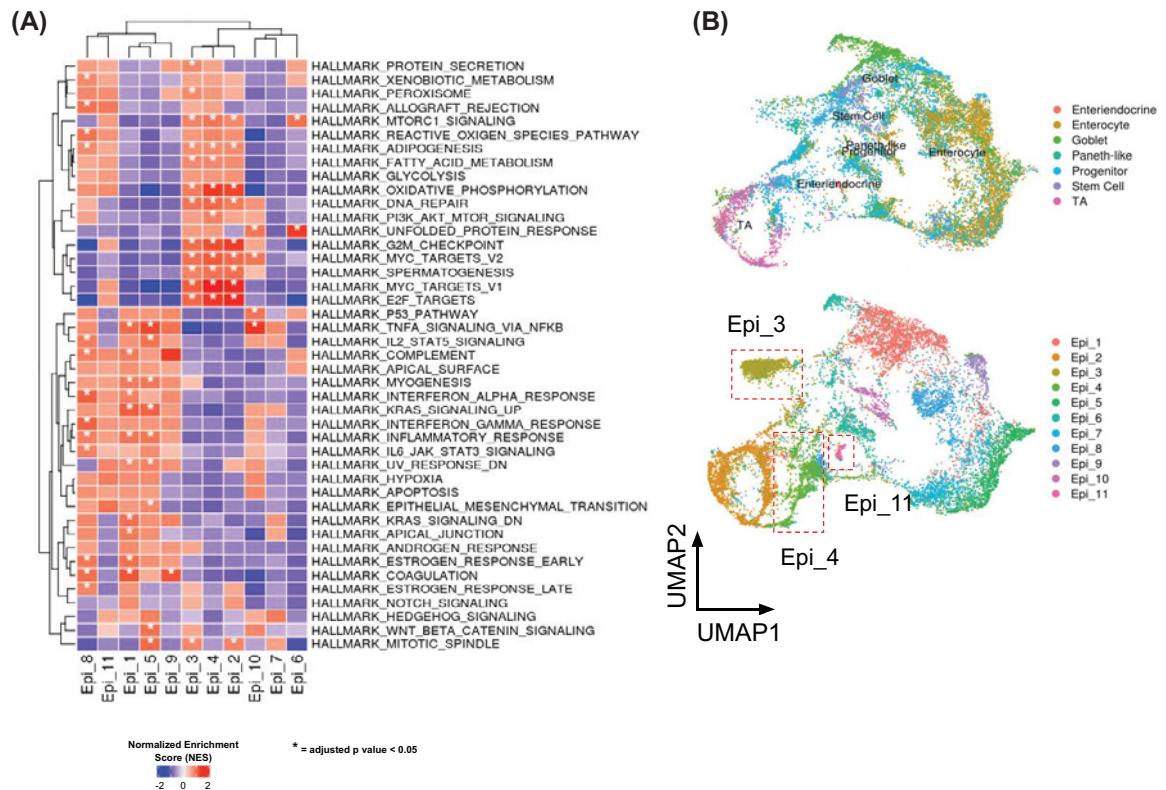


Figure 5. Functional gene set analysis of ascites-derived epithelial cells

(A) Heatmap showing the normalised enrichment score from GSEA of hallmark gene sets from MSigDB [35] (*, adjusted P -value < 0.05). Up-regulated genes in Epi.2, Epi.3, and Epi.4 were associated with hallmark gene sets in cell cycling, metabolism, and MTORC1 signaling pathways. (B) UMAP plot of integrated data between our malignant ascites single cell dataset and the normal gastrointestinal tract single cell dataset. Upper panel shows cells from normal gastrointestinal tract overlaid by original annotations. Lower panel shows epithelial subsets annotated as in Figure 4A. Epi.3 and Epi.4 showed slightest similarity when compared with normal gastrointestinal dataset.

in conjunction with cell type identification based on characterised molecular markers, we were able to identify different cell types in ascites as well as their relative abundances. While epithelial cells were the most abundant populations (66–95% of all the cells retrieved from the ascites samples, depending on the cell dissociation methods, and the sample collection time points in relation to the chemotherapy treatment), we also observed fractions of myeloid cells (1–33%), fibroblasts (0.2–0.9%), as well as other subpopulations that were present at lower abundance.

One of the most striking findings of this work is the extent to which the cell preparation methods, enzymatic and mechanical cell dissociation, affected not just the relative proportions of cell types in the ascites samples, but also on the transcriptomic profiles of these subpopulations. As shown in muscle stem cells, van den Brink and co-workers found that a widely used cell preparation protocol [56], which involves tissue dissociation by collagenase type II followed by fluorescence-activated cell sorting (FACS), could significantly induce transcriptional changes. The ‘immediate early genes’ (IEGs) appeared to be specifically up-regulated in a subset of enzymatically treated cells, which might reflect the artifacts from the dissociation protocol. Other studies that compared the effects of different enzymatic dissociation methods also observed the expression of the same IEGs when performing dissociation at 37°C [57–59]. Consistent with these earlier studies, we observed highly represented genes in the ascites samples prepared using enzymatic dissociation, e.g., *HES1*, *IER3*, *JUNB*, *IER2*, *SOCS3*, and *ID1*, which had been previously identified by van den Brink co-workers [56] and O’Flanagan co-workers [58]. In addition, we observed that the myeloid cells in our samples were markedly susceptible to enzymatic dissociation by Accumax, which contains proteolytic and collagenolytic enzymes, especially in the pre-treatment samples. To the best of our knowledge, there is no previous

report about the direct effect of enzymatic preparation on myeloid cells. Generally, this might be due to reduced cell viability after enzymatic treatment, plus cryopreservation.

Since our patient had been treated with mFOLFOX6 and CapeOx regimens before her ascites developed, this might have affected the viability of ascites-derived myeloid cell populations, resulting in more cell death after various manipulations. Moreover, as we observed the overall lower myeloid cell frequencies in the post-treatment ascites samples collected right after the first cycle of mFOLFIRI than in the pre-treatment samples regardless of preparation protocol, it is possible that this was the effect of cytotoxic chemotherapy-induced leukopenia. However, more careful investigations including further in-depth dissociation protocol comparisons for malignant ascites-derived cells are required to pinpoint the cause of this effect.

We compared the expression profiles of ascites-derived cells before and after a cycle of mFOLFIRI, comprising fluorouracil (5-FU), leucovorin, and irinotecan, which kill cancer cells via the inhibition of thymidylate synthase and topoisomerase I enzymes. However, due to the limitation of the sample size and sampling time points, it would be difficult to confidently investigate the specific impact of this chemotherapy regimen on the transcriptional changes and molecular pathways involved in the survival and progress of the cancerous cells. In spite of that, we have demonstrated the power of scRNA-seq in dissecting the heterogeneous subpopulations of metastasised cancer cells with distinct transcriptomic profiles. We have discovered that among the eleven epithelial subclusters, only three, namely Epi_9, Epi_10, Epi_11, seemed to be responsive to mFOLFIRI treatment, and one particular subcluster, Epi_3, could be considered a treatment-resistant population. This finding potentially reflects the poor outcome observed over this course of mFOLFIRI treatment in our patient.

We have also shown that these transcriptionally distinct cell populations also possessed unique functional characteristics, as the treatment-tolerant subpopulation, Epi_3, displayed the most divergent transcriptomic profile from that of any normal intestinal tissues. The cluster may represent a subclone with massive mutational events resulting in altered gene expression, which consequently allowed it to escape the chemotherapy treatment and became highly proliferated. Additionally, Epi_3 was uniquely enriched with genes in peroxisome pathways. Peroxisomes, which are reactive oxygen species (ROS)-degrading organelles, are known to play a role in therapeutic resistance in cancer when drugs inducing ROS-mediated apoptosis are involved [60], which is the case for both 5-FU and irinotecan [61,62]. On the contrary, the population of cells appeared to be the most susceptible to the treatment, Epi_9, Epi_10, and Epi_11, have relatively similar expression profiles as the normal enterocytes, progenitor cells, and normal enteroendocrine cells, respectively, which may explain why they are the most responsive to the cytotoxic treatment.

Taken together, we have provided one of the earliest studies where the groundbreaking scRNA-seq technology has been applied to explore the heterogeneity of the cells retrieved from malignant ascites. We have specifically demonstrated the cellular compositions of cell types found in the ascites samples, and showcased the under-appreciated impact of cell preparation protocols on the transcriptomic profiles of different cell types. Our results highlight the importance of using the optimised protocols in the scRNA-seq studies, and also emphasise the benefit of using scRNA-seq over the traditional bulk RNA-seq experiments, where the contributions to the overall expression from different cell types cannot be traced, in cancer research. Finally, we have provided an example of how scRNA-seq can be applied to routinely discarded ascites samples and resolve distinct subpopulations of cancer cells, in terms of both transcriptomic patterns, as well as cellular characteristics. Since malignant ascites is associated with advanced cancer and a poor prognosis, the potential usage of scRNA-seq to monitor real-time treatment response after chemotherapy initiation might help clinicians adjust or switch the regimens in a timely manner, which might extend the patients' overall survival. Also, the collective interpretation of gene expression profiles of each subcluster should provide a more accurate prognosis for the cancer patients than the currently used bulk RNA-seq data. Further studies will be required to comprehensively validate the applications of scRNA-seq to discover new predictive and prognostic biomarkers from malignant ascites and other specimen types, as well as explore new molecular mechanisms and treatment options of complex diseases such as cancers.

Data Availability

scRNA-seq data discussed in this publication have been deposited in NCBI's Gene Expression Omnibus and are accessible through the GEO Series accession number: GSE155953. All single-cell analyses and visualisations were performed in R version 3.6. Codes and scripts used in the bioinformatics analyses are available from the Github repository: <https://github.com/vclabsysbio/scRNAseq.CAascites>.

Competing Interests

The authors declare that there are no competing interests associated with the manuscript.

Funding

This work was supported by the Newton Advanced Fellowship through the Thailand Science Research and Innovation (TSRI) [grant number DBG60800003], the Royal Society [grant number NA160153]; the Mid-Career Researcher Grant from National Research Council of Thailand (NRCT) and Mahidol University [grant number NRCT5-RSA63015-24]; and the Program Management Unit for National Competitiveness Enhancement (PMU-C) [grant number C10F640057] (to Varodom Charoensawan); the Thailand Grand Challenge Program for Research University Network (RUN) under the Precision Medicine for Cancer Project by the National Research Council of Thailand (NRCT), and the Government Research Grant by the Health Systems Research Institute (HSRI) [grant number HSRI 63-140] (to Natini Jinawath). The Natini Jinawath and Varodom Charoensawan laboratories were supported by the Office of National Higher Education Science Research and Innovation Policy Council (NXPO) through the Integrative Computational BioScience (ICBS) Center, Mahidol University [grant number B05F630055].

CRedit Author Contribution

Tiraput Poonpanichakul: Formal analysis, Investigation, Visualisation, Writing—original draft, Writing—review & editing.

Meng-Shin Shiao: Investigation. **Natnicha Jiravejchakul:** Investigation. **Ponpan Matangkasombut:** Resources. **Ekapop**

Sirachainan: Resources, Writing—original draft. **Varodom Charoensawan:** Resources, Formal analysis, Supervision, Funding acquisition, Methodology, Writing—original draft, Writing—review & editing. **Natini Jinawath:** Resources, Formal analysis, Supervision, Funding acquisition, Methodology, Writing—original draft, Writing—review & editing.

Acknowledgements

We wholeheartedly thank the patient who contributed the samples for this research project. We thank the staff of Ramathibodi Tumor Biobank for sample collection and processing, and Dr Anunya Opasawatchai (Faculty of Dentistry, Mahidol University) for helpful suggestions about single-cell experiment and sample processing. Agilent TapeStation system for sample and library QC was supported by the Research Center, Faculty of Medicine Ramathibodi Hospital. Access to a High-Performance Computing (HPC) facility was provided by Integrative Computational BioScience (ICBS) Center, Mahidol University.

Abbreviations

CapeOx, capecitabine/oxaliplatin; CRC, colorectal cancer; CT, computed tomography; DEG, differentially expressed gene; FOLFIRI, a chemotherapy regimen consisting of leucovorin calcium (calcium folinate), 5-fluorouracil, and irinotecan; FOLFOX, a chemotherapy regimen that include leucovorin calcium (calcium folinate), 5-fluorouracil and oxaliplatin; GSEA, gene set enrichment analysis; IEG, immediate early gene; mFOLFIRI, modified FOLFIRI; mFOLFOX6, modified FOLFOX6; PBMC, peripheral blood mononuclear cell; RBC, red blood cell; rcf, relative centrifugal force; scRNA-seq, single-cell RNA-sequencing; UMAP, Uniform Manifold Approximation and Projection; 5-FU, fluorouracil.

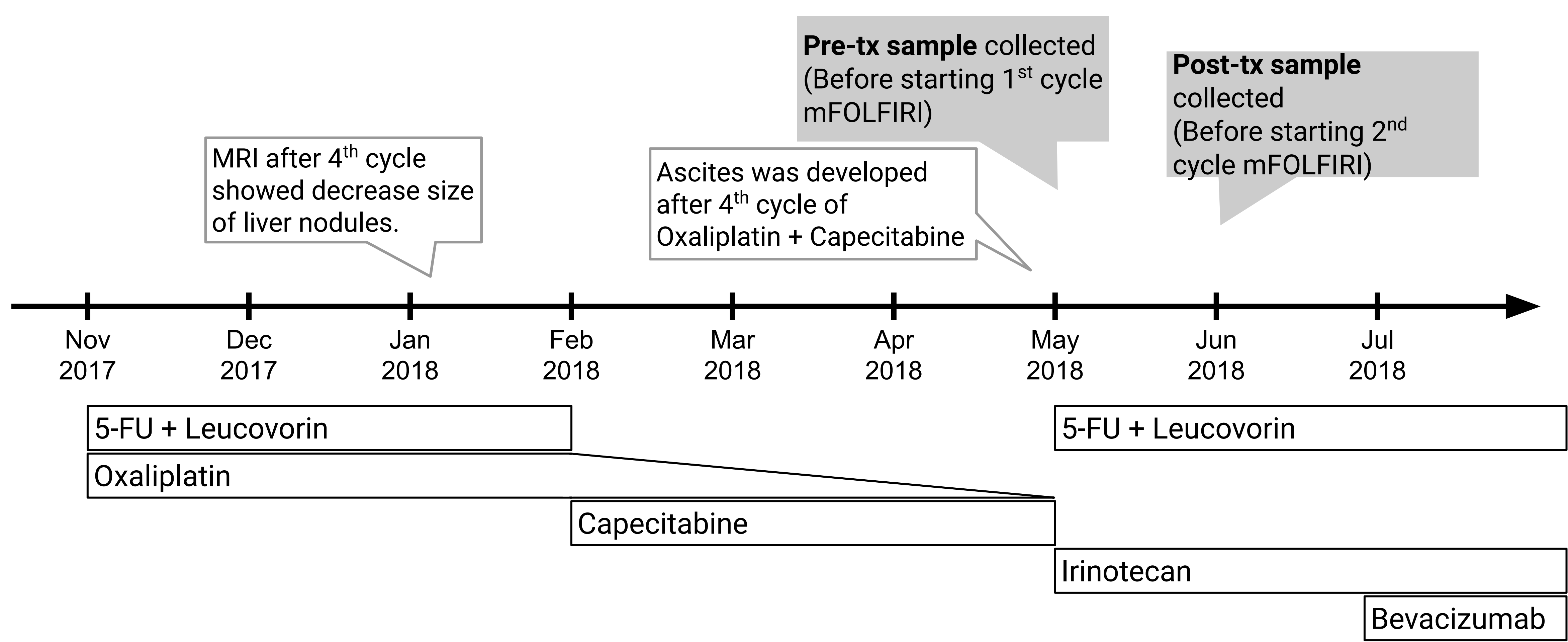
References

- Granados-Romero, J.J., Valderrama-Treviño, A.I., Contreras-Flores, E.H., Barrera-Mera, B., Herrera Enríquez, M., Uriarte-Ruiz, K. et al. (2017) Colorectal cancer: a review. *Int. J. Res. Med. Sci.* **5**, 4667, <https://doi.org/10.18203/2320-6012.ijrms20174914>
- Riihimäki, M., Hemminki, A., Sundquist, J. and Hemminki, K. (2016) Patterns of metastasis in colon and rectal cancer. *Sci. Rep.* **6**, 29765, <https://doi.org/10.1038/srep29765>
- Jacobson, R., Sherman, S.K., Dadaleh, F. and Turaga, K.K. (2018) Peritoneal metastases in colorectal cancer. *Ann. Surg. Oncol.* **25**, 2145–2151, <https://doi.org/10.1245/s10434-018-6490-x>
- Acharyya, S., Oskarsson, T., Vanharanta, S., Malladi, S., Kim, J., Morris, P.G. et al. (2012) A CXCL1 paracrine network links cancer chemoresistance and metastasis. *Cell* **150**, 165–178, <https://doi.org/10.1016/j.cell.2012.04.042>
- Kim, S., Lee, M., Dhanasekaran, D.N. and Song, Y.S. (2018) Activation of LXR α / β by cholesterol in malignant ascites promotes chemoresistance in ovarian cancer. *BMC Cancer* **18**, 1232, <https://doi.org/10.1186/s12885-018-5152-5>
- Walker, A.S., Zwintscher, N.P., Johnson, E.K., Maykel, J.A., Stojadinovic, A., Nissan, A. et al. (2014) Future directions for monitoring treatment response in colorectal cancer. *J. Cancer* **5**, 44–57, <https://doi.org/10.7150/jca.7809>
- Vogel, J.D., Eskicioglu, C., Weiser, M.R., Feingold, D.L. and Steele, S.R. (2017) The American Society of Colon and Rectal Surgeons Clinical Practice Guidelines for the treatment of colon cancer. *Dis. Colon Rectum* **60**, 999–1017, <https://doi.org/10.1097/DCR.0000000000000926>
- Van Cutsem, E., Cervantes, A., Nordlinger, B. and Arnold, D. (2014) Metastatic colorectal cancer: ESMO Clinical Practice Guidelines for diagnosis, treatment and follow-up. *Ann. Oncol.* **25**, iii1–iii9, <https://doi.org/10.1093/annonc/mdl260>
- Chiorean, E.G., Nandakumar, G., Fadelu, T., Temin, S., Alarcon-Rozas, A.E., Bejarano, S. et al. (2020) Treatment of patients with late-stage colorectal cancer: ASCO Resource-Stratified Guideline. *JCO Glob. Oncol.* **6**, 414–438, <https://doi.org/10.1200/JGO.19.00367>
- Song, S.E., Choi, P., Kim, J.H., Jung, K., Kim, S.E., Moon, W. et al. (2018) Diagnostic value of carcinoembryonic antigen in ascites for colorectal cancer with peritoneal carcinomatosis. *Korean J. Gastroenterol.* **71**, 332–337, <https://doi.org/10.4166/kjg.2018.71.6.332>
- Choi, D.-S., Park, J.O., Jang, S.C., Yoon, Y.J., Jung, J.W., Choi, D.-Y. et al. (2011) Proteomic analysis of microvesicles derived from human colorectal cancer ascites. *Proteomics* **11**, 2745–2751, <https://doi.org/10.1002/pmic.201100022>

- 12 Latifi, A., Luwor, R.B., Bilandzic, M., Nazaretian, S., Stenvers, K., Pyman, J. et al. (2012) Isolation and characterization of tumor cells from the ascites of ovarian cancer patients: molecular phenotype of chemoresistant ovarian tumors. *PLoS ONE* **7**, e46858, <https://doi.org/10.1371/journal.pone.0046858>
- 13 Kim, S., Kim, B. and Song, Y.S. (2016) Ascites modulates cancer cell behavior, contributing to tumor heterogeneity in ovarian cancer. *Cancer Sci.* **107**, 1173–1178, <https://doi.org/10.1111/cas.12987>
- 14 Guinney, J., Dienstmann, R., Wang, X., de Reyniès, A., Schlicker, A., Soneson, C. et al. (2015) The consensus molecular subtypes of colorectal cancer. *Nat. Med.* **21**, 1350–1356, <https://doi.org/10.1038/nm.3967>
- 15 Molinari, C., Marisi, G., Passardi, A., Matteucci, L., De Maio, G. and Ulivi, P. (2018) Heterogeneity in colorectal cancer: a challenge for personalized medicine? *Int. J. Mol. Sci.* **19**, 3733, <https://doi.org/10.3390/ijms19123733>
- 16 Punt, C.J.A., Koopman, M. and Vermeulen, L. (2017) From tumour heterogeneity to advances in precision treatment of colorectal cancer. *Nat. Rev. Clin. Oncol.* **14**, 235–246, <https://doi.org/10.1038/nrclinonc.2016.171>
- 17 Shalek, A.K. and Benson, M. (2017) Single-cell analyses to tailor treatments. *Sci. Transl. Med.* **9**, eaan4730, <https://doi.org/10.1126/scitranslmed.aan4730>
- 18 Levitin, H.M., Yuan, J. and Sims, P.A. (2018) Single-cell transcriptomic analysis of tumor heterogeneity. *Trends Cancer* **4**, 264–268, <https://doi.org/10.1016/j.trecan.2018.02.003>
- 19 Valdes-Mora, F., Handler, K., Law, A.M.K., Salomon, R., Oakes, S.R., Ormandy, C.J. et al. (2018) Single-cell transcriptomics in cancer immunobiology: the future of precision oncology. *Front. Immunol.* **9**, 2582, <https://doi.org/10.3389/fimmu.2018.02582>
- 20 Tieng, F.Y.F., Baharudin, R., Abu, N., Mohd Yunus, R.-I., Lee, L.-H. and Ab Mutalib, N.-S. (2020) Single cell transcriptome in colorectal cancer—current updates on its application in metastasis, chemoresistance and the roles of circulating tumor cells. *Front. Pharmacol.* **11**, 135, <https://doi.org/10.3389/fphar.2020.00135>
- 21 Kyrochristos, I.D., Zioqas, D.E., Goussia, A., Glantzounis, G.K. and Roukos, D.H. (2019) Bulk and single-cell next-generation sequencing: individualizing treatment for colorectal cancer. *Cancers* **11**, 1809, <https://doi.org/10.3390/cancers11111809>
- 22 Li, H., Courtois, E.T., Sengupta, D., Tan, Y., Chen, K.H., Goh, J.J.L. et al. (2017) Reference component analysis of single-cell transcriptomes elucidates cellular heterogeneity in human colorectal tumors. *Nat. Genet.* **49**, 708–718, <https://doi.org/10.1038/ng.3818>
- 23 Dai, W., Zhou, F., Tang, D., Lin, L., Zou, C., Tan, W. et al. (2019) Single-cell transcriptional profiling reveals the heterogeneity in colorectal cancer. *Medicine (Baltimore)* **98**, e16916
- 24 Tang-Huau, T.-L., Gueguen, P., Goudot, C., Durand, M., Bohec, M., Baulande, S. et al. (2018) Human in vivo-generated monocyte-derived dendritic cells and macrophages cross-present antigens through a vacuolar pathway. *Nat. Commun.* **9**, 2570, <https://doi.org/10.1038/s41467-018-04985-0>
- 25 Andrews, S. (2010) FastQC: a quality control tool for high throughput sequence data. <https://www.bioinformatics.babraham.ac.uk/projects/fastqc/>
- 26 Stuart, T., Butler, A., Hoffman, P., Hafemeister, C., Papalexi, E., Mauck, W.M. et al. (2019) Comprehensive integration of single-cell data. *Cell* **177**, 1888.e21–1902.e21, <https://doi.org/10.1016/j.cell.2019.05.031>
- 27 Young, M.D. and Behjati, S. (2020) SoupX removes ambient RNA contamination from droplet-based single-cell RNA sequencing data. *GigaScience* **9**, g1aa151, <https://doi.org/10.1093/gigascience/g1aa151>
- 28 McGinnis, C.S., Murrow, L.M. and Gartner, Z.J. (2019) DoubletFinder: doublet detection in single-cell RNA sequencing data using artificial nearest neighbors. *Cell Syst.* **8**, 329.e4–337.e4, <https://doi.org/10.1016/j.cels.2019.03.003>
- 29 Hafemeister, C. and Satija, R. (2019) Normalization and variance stabilization of single-cell RNA-seq data using regularized negative binomial regression. *Genome Biol.* **20**, 296, <https://doi.org/10.1186/s13059-019-1874-1>
- 30 McInnes, L., Healy, J. and Melville, J. (2018) UMAP: Uniform Manifold Approximation and Projection for Dimension Reduction. *arXiv*, <http://arxiv.org/abs/1802.03426>
- 31 Traag, V.A., Waltman, L. and van Eck, N.J. (2019) From Louvain to Leiden: guaranteeing well-connected communities. *Sci. Rep.* **9**, 5233, <https://doi.org/10.1038/s41598-019-41695-z>
- 32 Gu, Z., Eils, R. and Schlesner, M. (2016) Complex heatmaps reveal patterns and correlations in multidimensional genomic data. *Bioinformatics* **32**, 2847–2849, <https://doi.org/10.1093/bioinformatics/btw313>
- 33 Subramanian, A., Tamayo, P., Mootha, V.K., Mukherjee, S., Ebert, B.L., Gillette, M.A. et al. (2005) Gene set enrichment analysis: A knowledge-based approach for interpreting genome-wide expression profiles. *Proc. Natl. Acad. Sci. U.S.A.* **102**, 15545–15550, <https://doi.org/10.1073/pnas.0506580102>
- 34 Korotkevich, G., Sukhov, V. and Sergushichev, A. (2016) Fast gene set enrichment analysis. *bioRxiv*, <https://doi.org/10.1101/060012>
- 35 Liberzon, A., Birger, C., Thorvaldsdóttir, H., Ghandi, M., Mesirov, J.P. and Tamayo, P. (2015) The Molecular Signatures Database Hallmark Gene Set Collection. *Cell Syst.* **1**, 417–425, <https://doi.org/10.1016/j.cels.2015.12.004>
- 36 Wang, Y., Song, W., Wang, J., Wang, T., Xiong, X., Qi, Z. et al. (2020) Single-cell transcriptome analysis reveals differential nutrient absorption functions in human intestine. *J. Exp. Med.* **217**, e20191130, <https://doi.org/10.1084/jem.20191130>
- 37 Croix BST (2000) Genes expressed in human tumor endothelium. *Science* **289**, 1197–1202, <https://doi.org/10.1126/science.289.5482.1197>
- 38 Zhang, C., Lu, L., Li, Y., Wang, X., Zhou, J., Liu, Y. et al. (2012) IGF binding protein-6 expression in vascular endothelial cells is induced by hypoxia and plays a negative role in tumor angiogenesis. *Int. J. Cancer* **130**, 2003–2012, <https://doi.org/10.1002/ijc.26201>
- 39 Liao, Y., Lei, J., Liu, M., Lin, W., Hong, D., Tuo, Y. et al. (2016) Mesenchymal stromal cells mitigate experimental colitis via insulin-like growth factor binding protein 7-mediated immunosuppression. *Mol. Ther.* **24**, 1860–1872, <https://doi.org/10.1038/mt.2016.140>
- 40 Jiang, B.-H. and Liu, L.-Z. (2008) Role of mTOR in anticancer drug resistance: perspectives for improved drug treatment. *Drug Resist. Updat.* **11**, 63–76
- 41 Hsu, Y.-C., Li, L. and Fuchs, E. (2014) Transit-amplifying cells orchestrate stem cell activity and tissue regeneration. *Cell* **157**, 935–949, <https://doi.org/10.1016/j.cell.2014.02.057>

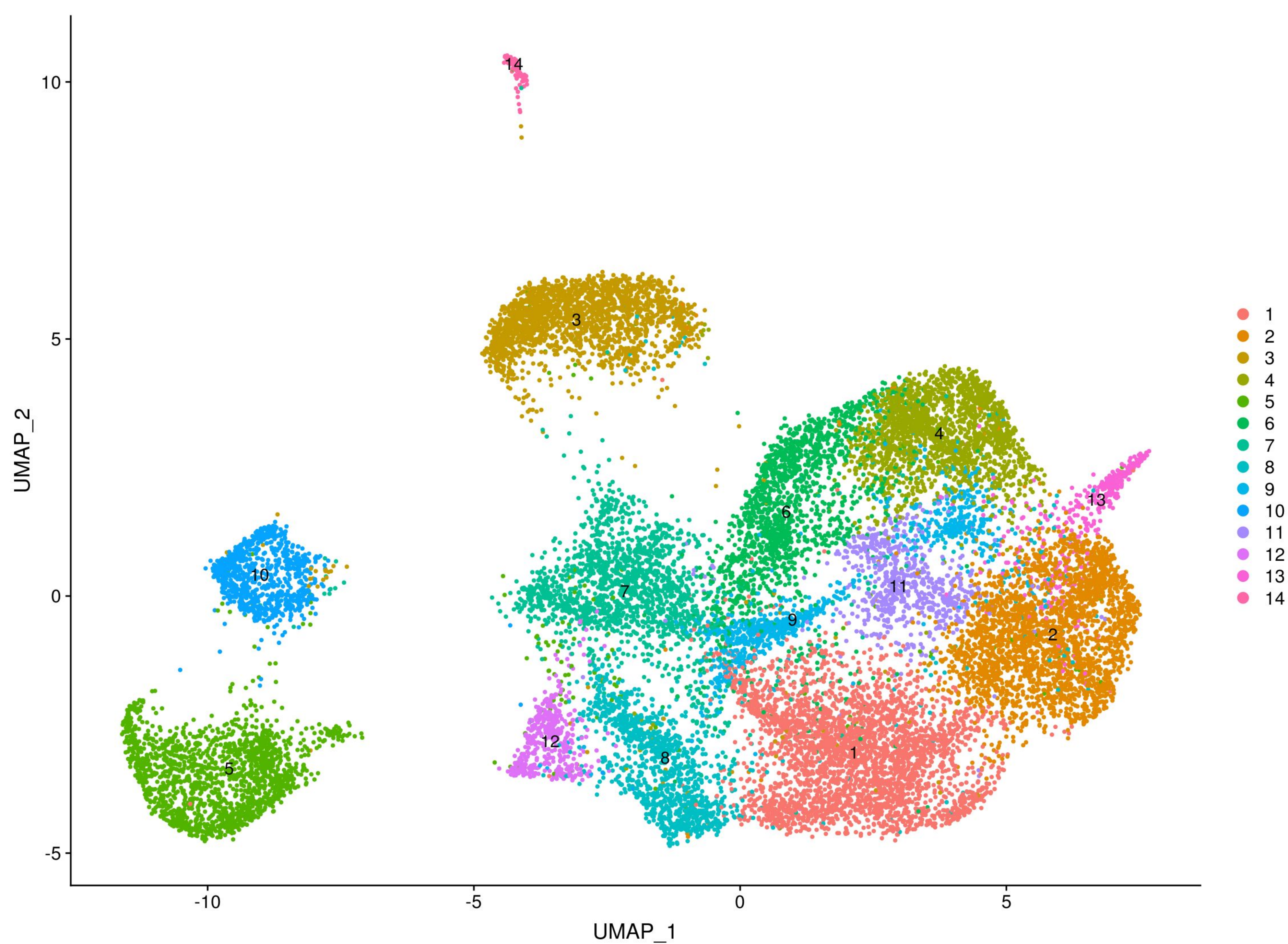
- 42 Gehart, H. and Clevers, H. (2019) Tales from the crypt: new insights into intestinal stem cells. *Nat. Rev. Gastroenterol. Hepatol.* **16**, 19–34, <https://doi.org/10.1038/s41575-018-0081-y>
- 43 Svensson, V., Vento-Tormo, R. and Teichmann, S.A. (2018) Exponential scaling of single-cell RNA-seq in the past decade. *Nat. Protoc.* **13**, 599–604, <https://doi.org/10.1038/nprot.2017.149>
- 44 Zhang, Y., Song, J., Zhao, Z., Yang, M., Chen, M., Liu, C. et al. (2020) Single-cell transcriptome analysis reveals tumor immune microenvironment heterogeneity and granulocytes enrichment in colorectal cancer liver metastases. *Cancer Lett.* **470**, 84–94, <https://doi.org/10.1016/j.canlet.2019.10.016>
- 45 Dai, W., Zhou, F., Tang, D., Lin, L., Zou, C., Tan, W. et al. (2019) Single-cell transcriptional profiling reveals the heterogeneity in colorectal cancer. *Medicine (Baltimore)* **98**, e16916, <https://doi.org/10.1097/MD.00000000000016916>
- 46 Ono, H., Arai, Y., Furukawa, E., Narushima, D., Matsuura, T., Nakamura, H. et al. (2019) Single-cell DNA and RNA sequencing reveals the dynamics of intra-tumor heterogeneity in a colorectal cancer model. *bioRxiv*, <https://doi.org/10.1101/616870>
- 47 Chen, K.-Y., Srinivasan, T., Lin, C., Tung, K.-L., Gao, Z. and Hsu, D.S. (2018) Single-cell transcriptomics reveals heterogeneity and drug response of human colorectal cancer organoids. *2018 40th Annual International Conference of the IEEE Engineering in Medicine and Biology Society (EMBC)*, pp. 2378–2381, IEEE, Honolulu, HI, <https://ieeexplore.ieee.org/document/8512784/>
- 48 Bian, S., Hou, Y., Zhou, X., Li, X., Yong, J., Wang, Y. et al. (2018) Single-cell multiomics sequencing and analyses of human colorectal cancer. *Science* **362**, 1060–1063, <https://doi.org/10.1126/science.aao3791>
- 49 Choi, D.-S., Park, J.O., Jang, S.C., Yoon, Y.J., Jung, J.W., Choi, D.-Y. et al. (2011) Proteomic analysis of microvesicles derived from human colorectal cancer ascites. *Proteomics* **11**, 2745–2751, <https://doi.org/10.1002/pmic.201100022>
- 50 Peterson, V.M., Castro, C.M., Chung, J., Miller, N.C., Ullal, A.V., Castano, M.D. et al. (2013) Ascites analysis by a microfluidic chip allows tumor-cell profiling. *Proc. Natl. Acad. Sci. U.S.A.* **110**, E4978–E4986, <https://doi.org/10.1073/pnas.1315370110>
- 51 Golan, T., Eckhardt, S.G., Stossel, C., Atlas, D., Wang, G., Pitts, T.M. et al. (2014) RNA-seq and KRAS mutational status in ascitic pancreatic cancer cells: novel results and distinct subsets. *J. Clin. Oncol.* **32**, e15214, <https://doi.org/10.1200/jco.2014.32.15.suppl.e15214>
- 52 Ahmed, N., Greening, D., Samardzija, C., Escalona, R.M., Chen, M., Findlay, J.K. et al. (2016) Unique proteome signature of post-chemotherapy ovarian cancer ascites-derived tumor cells. *Sci. Rep.* **6**, 30061, <https://doi.org/10.1038/srep30061>
- 53 Li, X., Zhu, D., Li, N., Yang, H., Zhao, Z. and Li, M. (2017) Characterization of ascites-derived tumor cells from an endometrial cancer patient. *Cancer Sci.* **108**, 2352–2357, <https://doi.org/10.1111/cas.13407>
- 54 Schelker, M., Feau, S., Du, J., Ranu, N., Klipp, E., MacBeath, G. et al. (2017) Estimation of immune cell content in tumour tissue using single-cell RNA-seq data. *Nat. Commun.* **8**, 2032, <https://doi.org/10.1038/s41467-017-02289-3>
- 55 Hu, Y., Qi, C., Liu, X., Zhang, C., Gao, J., Wu, Y. et al. (2019) Malignant ascites-derived exosomes promote peritoneal tumor cell dissemination and reveal a distinct miRNA signature in advanced gastric cancer. *Cancer Lett.* **457**, 142–150, <https://doi.org/10.1016/j.canlet.2019.04.034>
- 56 van den Brink, S.C., Sage, F., Vártesy, Á., Spanjaard, B., Peterson-Maduro, J., Baron, C.S. et al. (2017) Single-cell sequencing reveals dissociation-induced gene expression in tissue subpopulations. *Nat. Methods* **14**, 935–936, <https://doi.org/10.1038/nmeth.4437>
- 57 Adam, M., Potter, A.S. and Potter, S.S. (2017) Psychrophilic proteases dramatically reduce single-cell RNA-seq artifacts: a molecular atlas of kidney development. *Development* **144**, 3625–3632
- 58 O'Flanagan, C.H., Campbell, K.R., Zhang, A.W., Kabeer, F., Lim, J.L.P., Biele, J. et al. (2019) Dissociation of solid tumor tissues with cold active protease for single-cell RNA-seq minimizes conserved collagenase-associated stress responses. *Genome Biol.* **20**, 210, <https://doi.org/10.1186/s13059-019-1830-0>
- 59 Denisenko, E., Guo, B.B., Jones, M., Hou, R., de Kock, L., Lassmann, T. et al. (2020) Systematic assessment of tissue dissociation and storage biases in single-cell and single-nucleus RNA-seq workflows. *Genome Biol.* **21**, 130, <https://doi.org/10.1186/s13059-020-02048-6>
- 60 Islinger, M., Voelkl, A., Fahimi, H.D. and Schrader, M. (2018) The peroxisome: an update on mysteries 2.0. *Histochem. Cell Biol.* **150**, 443–471, <https://doi.org/10.1007/s00418-018-1722-5>
- 61 Hwang, I.T., Chung, Y.M., Kim, J.J., Chung, J.S., Kim, B.S., Kim, H.J. et al. (2007) Drug resistance to 5-FU linked to reactive oxygen species modulator 1. *Biochem. Biophys. Res. Commun.* **359**, 304–310, <https://doi.org/10.1016/j.bbrc.2007.05.088>
- 62 Huang, Y.-F., Zhu, D.-J., Chen, X.-W., Chen, Q.-K., Luo, Z.-T., Liu, C.-C. et al. (2017) Curcumin enhances the effects of irinotecan on colorectal cancer cells through the generation of reactive oxygen species and activation of the endoplasmic reticulum stress pathway. *Oncotarget* **8**, 40264–40275, <https://doi.org/10.18632/oncotarget.16828>

Supplementary Figure 1



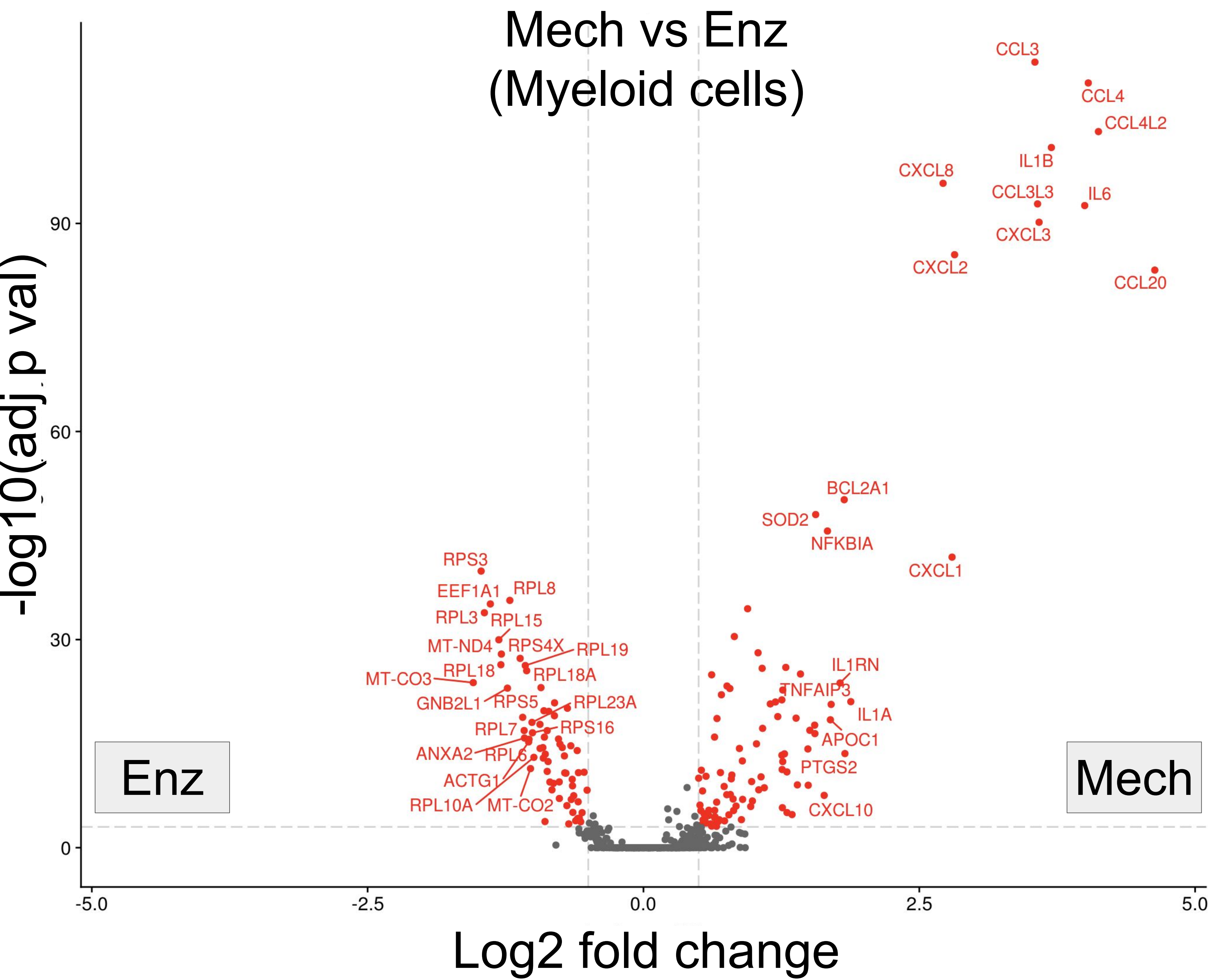
Supplementary Figure 1. A flowchart shows the complete timeline of treatment, clinical investigations, and clinical course of the patient in this study.

Supplementary Figure 2



Supplementary Figure 2. UMAP plot showing the original Leiden clustering of the 14 sub-clusters of integrated data.

Supplementary Figure 3



Supplementary Figure 3. Volcano plot showing DEGs from the comparison between mechanical and enzymatic preparations of myeloid cells. Colored dots highlighted genes that have log 2 fold change > 0.5 and adjusted p-value < 0.01.

Supplementary Table 1. Summary metric of scRNA-seq data output after read mapping and UMI quantification using Cellranger pipeline.

	CCM-B	CCM-A	CCE-B	CCE-A
	Mech Pre-tx	Mech Post-tx	Enz Pre-tx	Enz Post-tx
Estimated Number of Cells	4,984	3,580	5,824	7,694
Mean Reads per Cell	41,940	62,594	37,882	28,570
Median Genes per Cell	1,685	3,076	2,528	2,388
Number of Reads	209,033,934	224,087,238	220,629,775	219,824,446
Valid Barcodes	97.80%	96.90%	97.90%	96.90%
Sequencing Saturation	60.00%	39.60%	55.80%	33.60%
Q30 Bases in Barcode	96.90%	97.30%	96.80%	97.30%
Q30 Bases in RNA Read	89.00%	90.90%	88.10%	90.80%
Q30 Bases in Sample Index	95.20%	95.30%	95.10%	95.50%
Q30 Bases in UMI	96.80%	97.20%	96.70%	97.20%
Reads Mapped to Genome	95.30%	97.20%	94.50%	97.30%
Reads Mapped Confidently to Genome	92.90%	95.10%	92.10%	95.20%
Reads Mapped Confidently to Intergenic Regions	3.20%	2.40%	2.90%	2.50%
Reads Mapped Confidently to Intronic Regions	11.90%	8.60%	11.80%	11.70%
Reads Mapped Confidently to Exonic Regions	77.80%	84.10%	77.40%	81.00%
Reads Mapped Confidently to Transcriptome	73.40%	79.40%	73.10%	76.60%
Reads Mapped Antisense to Gene	1.30%	1.20%	1.10%	1.30%
Fraction Reads in Cells	91.30%	76.00%	94.40%	87.90%
Total Genes Detected	21,833	21,766	21,713	21,929
Median UMI Counts per Cell	5,017	12,250	9,217	7,005

Supplementary Table 2. List of DEGs from the comparison between mechanical and enzymatic dissociations of epithelial cells (log2 fold change > 0.1).

gene	log2_avgFC	p_val_adj	pct.1	pct.2
CD81	0.5367	4.76E-171	0.57	0.377
PPP1CB	0.5152	1.14E-62	0.495	0.38
HNRNPH1	0.4667	8.75E-63	0.258	0.15
RPL41	0.3324	1.73E-136	0.913	0.885
RPS10	0.3172	6.84E-78	0.758	0.699
HSPA1B	0.3113	7.18E-01	0.412	0.372
IFI6	0.2986	3.67E-10	0.643	0.609
TIMP2	0.2881	3.15E-86	0.557	0.386
CTTN	0.2534	8.36E-46	0.512	0.377
RPS17	0.2514	2.14E-104	0.894	0.875
RPL26	0.2442	1.69E-68	0.903	0.885
FTL	0.2366	1.51E-07	0.932	0.947
PSMA2	0.2364	6.93E-33	0.587	0.474
NDUFA11	0.2335	1.30E-40	0.691	0.6
HLA-B	0.2314	1.98E-04	0.752	0.729
RPL35A	0.2297	1.59E-101	0.917	0.9
PPP3CA	0.2290	2.36E-20	0.262	0.191
TOMM7	0.2238	4.18E-42	0.752	0.698
C15orf48	0.2235	1.51E-02	0.468	0.431
RPL23A	0.2223	1.45E-104	0.934	0.931
RPS12	0.2170	6.25E-155	0.95	0.95
ZFAND2A	0.2134	5.66E-12	0.262	0.202
ZFAS1	0.2129	1.13E-14	0.736	0.69
NDUFA13	0.2097	8.70E-33	0.638	0.529
TRA2A	0.2070	7.64E-51	0.29	0.178
RPL21	0.2047	1.12E-30	0.899	0.879
RPL27	0.2045	1.75E-80	0.885	0.877
SNHG8	0.2021	6.14E-20	0.425	0.336
HSPA1A	0.1985	1.00E+00	0.336	0.308
COMMD6	0.1975	2.07E-34	0.717	0.641
IFI27	0.1961	4.18E-30	0.866	0.862
UQCR11	0.1960	1.18E-36	0.783	0.74
RPS25	0.1952	4.41E-76	0.926	0.918
RPS15A	0.1951	1.11E-75	0.92	0.902
FTH1	0.1949	1.07E-09	0.982	0.992
WTAP	0.1922	1.80E-20	0.289	0.211
COX7A2	0.1908	5.52E-45	0.814	0.794

SEC61G	0.1898	3.31E-21	0.768	0.737
FXVD3	0.1841	4.90E-12	0.659	0.598
UBA52	0.1817	1.14E-79	0.894	0.886
C6orf48	0.1790	3.40E-12	0.525	0.448
NDUFB2	0.1788	6.69E-25	0.77	0.743
RPL34	0.1760	2.48E-65	0.921	0.915
RARRES3	0.1737	3.27E-05	0.485	0.426
RPL28	0.1734	7.29E-88	0.943	0.94
ADIRF	0.1708	6.03E-23	0.856	0.851
SNHG7	0.1707	1.48E-12	0.525	0.445
RPL36A	0.1706	4.07E-29	0.761	0.663
OST4	0.1704	8.09E-32	0.787	0.765
SKP1	0.1667	6.52E-15	0.716	0.66
RPS13	0.1636	3.03E-61	0.899	0.897
RPS28	0.1629	1.66E-62	0.912	0.897
RPL35	0.1627	2.40E-56	0.921	0.915
MINOS1	0.1621	9.52E-20	0.651	0.585
S100A2	0.1620	4.75E-07	0.491	0.427
MRPL33	0.1613	3.04E-28	0.644	0.536
SERPINA1	0.1606	3.99E-04	0.329	0.282
B2M	0.1599	6.85E-04	0.91	0.912
RPLP2	0.1597	1.51E-82	0.96	0.959
TMEM59	0.1594	8.59E-17	0.604	0.509
RPL30	0.1587	9.40E-70	0.908	0.91
COX8A	0.1518	3.85E-23	0.757	0.731
TMED4	0.1509	3.31E-19	0.426	0.33
COX7C	0.1497	3.07E-26	0.833	0.817
RPL17	0.1486	2.86E-18	0.593	0.503
SAR1A	0.1485	4.02E-18	0.482	0.379
ITM2B	0.1484	8.09E-11	0.524	0.429
ARPC4	0.1481	1.35E-26	0.495	0.377
RPS27A	0.1471	5.43E-52	0.944	0.944
RPS21	0.1464	9.69E-28	0.834	0.816
POLR2L	0.1439	1.50E-13	0.76	0.73
MYEOV2	0.1430	2.18E-16	0.63	0.549
C4orf3	0.1421	5.08E-11	0.633	0.565
ATP5E	0.1399	2.60E-25	0.823	0.8
DNAJB1	0.1386	1.00E+00	0.564	0.526
UBL5	0.1381	1.54E-17	0.78	0.741
RPL27A	0.1378	2.69E-63	0.952	0.959
EIF2S3	0.1371	7.53E-30	0.496	0.376
BTG1	0.1354	1.00E+00	0.4	0.36
SMIM22	0.1354	7.06E-25	0.543	0.428
RPS19	0.1353	1.02E-66	0.968	0.974
LCN2	0.1347	1.00E+00	0.772	0.773
ATP5G2	0.1346	6.55E-13	0.725	0.683
RPLP1	0.1343	5.64E-51	0.962	0.97
BLOC1S1	0.1339	1.14E-19	0.541	0.443
TMEM256	0.1330	1.17E-30	0.482	0.36
RPS8	0.1330	8.06E-59	0.936	0.937
PARD6B	0.1322	2.45E-20	0.264	0.186

BLVRB	0.1314	7.25E-10	0.607	0.528
RPL32	0.1312	1.87E-56	0.953	0.96
ATP5J2	0.1311	2.45E-14	0.783	0.776
SNRPD2	0.1302	5.87E-11	0.751	0.711
RPL31	0.1293	8.88E-43	0.927	0.932
C12orf57	0.1292	7.08E-20	0.471	0.371
NDUFA1	0.1280	2.81E-16	0.723	0.651
RPS23	0.1280	1.14E-56	0.93	0.93
TSTD1	0.1278	2.62E-12	0.663	0.596
HERPUD1	0.1275	3.86E-06	0.287	0.234
HLA-A	0.1271	1.00E+00	0.814	0.805
RPL36	0.1263	1.22E-50	0.936	0.93
HPGD	0.1261	1.00E+00	0.653	0.636
RPS14	0.1238	2.30E-65	0.945	0.95
RPS26	0.1235	8.13E-25	0.816	0.808
RPS15	0.1235	9.39E-46	0.963	0.966
METRNL	0.1235	1.48E-20	0.262	0.192
RPS24	0.1234	3.34E-11	0.92	0.914
NDUFB4	0.1229	1.17E-12	0.743	0.713
RPS16	0.1220	4.74E-47	0.927	0.93
RPS20	0.1216	5.87E-38	0.907	0.905
ATOX1	0.1214	8.05E-14	0.575	0.489
IFI27L2	0.1212	2.51E-22	0.381	0.282
EIF5	0.1211	1.14E-10	0.609	0.52
RPL37A	0.1205	9.54E-32	0.868	0.863
NDUFA4	0.1187	1.08E-10	0.76	0.753
AXL	0.1185	2.21E-20	0.294	0.216
RPS18	0.1185	3.69E-55	0.974	0.982
MRPL52	0.1183	2.55E-17	0.595	0.499
CD47	0.1182	3.32E-13	0.399	0.317
IL18	0.1182	2.89E-03	0.654	0.605
MIA	0.1182	6.52E-21	0.405	0.308
TMSB10	0.1177	1.84E-20	0.961	0.968
RPL39	0.1175	1.92E-41	0.932	0.911
HINT1	0.1167	4.03E-12	0.799	0.78
TCEB2	0.1164	1.52E-18	0.809	0.801
RPL22	0.1162	7.08E-18	0.862	0.857
XBP1	0.1154	3.13E-04	0.351	0.291
RPL13A	0.1150	4.91E-28	0.952	0.961
RPS27L	0.1148	8.29E-12	0.574	0.488
CHCHD1	0.1142	1.23E-07	0.558	0.484
IAH1	0.1142	5.52E-11	0.551	0.462
MALAT1	0.1140	1.51E-03	0.878	0.915
SET	0.1140	9.37E-02	0.739	0.71
ZRANB2	0.1126	1.27E-22	0.392	0.286
HSPB1	0.1115	1.00E+00	0.855	0.855
LAMTOR2	0.1108	1.06E-15	0.569	0.47
MDK	0.1096	1.55E-06	0.468	0.4
PIN4	0.1094	2.85E-22	0.431	0.322
TCEAL4	0.1086	5.33E-22	0.438	0.33
BST2	0.1082	1.44E-03	0.486	0.431
RPS27	0.1081	2.62E-42	0.912	0.901

RNF181	0.1074	2.39E-08	0.489	0.41
NDUFB8	0.1073	2.38E-08	0.672	0.61
DBI	0.1067	3.73E-14	0.49	0.393
HSPA8	0.1059	1.54E-09	0.749	0.69
RPL12	0.1059	8.28E-18	0.939	0.947
PET100	0.1052	7.86E-22	0.461	0.343
RPL10A	0.1051	1.37E-22	0.892	0.889
TMEM258	0.1046	1.92E-13	0.764	0.73
SREK1IP1	0.1045	7.47E-20	0.333	0.24
VAMP8	0.1044	1.27E-06	0.535	0.466
FAU	0.1038	4.82E-36	0.907	0.913
KTN1	0.1037	4.03E-06	0.658	0.575
TAF1D	0.1034	1.15E-09	0.591	0.502
AIMP1	0.1033	2.50E-09	0.587	0.494
SERF2	0.1033	1.11E-11	0.848	0.857
S100A6	0.1032	2.78E-41	0.963	0.973
HBA1	0.1031	1.76E-12	0.329	0.258
ANAPC16	0.1031	1.09E-08	0.637	0.556
RP11-357H14.17	0.1031	2.09E-06	0.536	0.456
RABAC1	0.1030	2.98E-06	0.6	0.528
N4BP2L2	0.1018	7.91E-11	0.31	0.237
RPS5	0.1014	1.02E-18	0.903	0.908
PSME1	0.1008	4.60E-03	0.656	0.591
EIF3E	0.1007	5.09E-01	0.779	0.733
SND1	-0.1002	1.00E+00	0.315	0.312
IQGAP1	-0.1002	1.00E+00	0.363	0.32
TMEM123	-0.1003	2.17E-05	0.806	0.81
H1F0	-0.1006	1.00E+00	0.443	0.415
MAD2L1	-0.1007	1.00E+00	0.356	0.354
PARP1	-0.1008	1.00E+00	0.38	0.359
TSSC1	-0.1008	1.00E+00	0.385	0.356
TRIP6	-0.1011	1.00E+00	0.445	0.413
KLF6	-0.1016	1.07E-05	0.752	0.756
EWSR1	-0.1018	1.00E+00	0.42	0.393
PTGES2	-0.1021	1.00E+00	0.477	0.436
PSMD3	-0.1023	1.00E+00	0.539	0.496
VASP	-0.1027	1.00E+00	0.379	0.37
IFRD2	-0.1029	1.00E+00	0.437	0.405
IFT57	-0.1030	1.00E+00	0.267	0.248
BMP7	-0.1030	1.00E+00	0.324	0.298
AGPAT2	-0.1032	1.00E+00	0.59	0.544
CFL1	-0.1034	4.20E-11	0.83	0.847
BRD4	-0.1034	1.00E+00	0.377	0.351
MCM3	-0.1036	1.00E+00	0.281	0.242
SPAG7	-0.1037	2.46E-01	0.278	0.294
MYH9	-0.1037	1.00E+00	0.4	0.366
GNB1	-0.1037	1.00E+00	0.429	0.381
DNPEP	-0.1037	2.81E-03	0.329	0.343
TMEM11	-0.1039	1.00E+00	0.287	0.279
ASAP2	-0.1041	2.68E-01	0.355	0.355
MT-ND4	-0.1041	1.00E+00	0.791	0.847

ENTPD6	-0.1043	1.00E+00	0.324	0.309
RNF126	-0.1044	1.00E+00	0.483	0.449
CALU	-0.1044	1.00E+00	0.507	0.475
MRPS26	-0.1045	1.00E+00	0.541	0.501
PGM2L1	-0.1045	1.00E+00	0.285	0.274
TNFRSF1A	-0.1045	1.00E+00	0.308	0.308
RRP9	-0.1047	1.00E+00	0.297	0.285
PLOD1	-0.1048	1.00E+00	0.269	0.266
WIPI2	-0.1049	1.00E+00	0.363	0.339
RALY	-0.1051	3.65E-01	0.526	0.497
LBR	-0.1052	1.00E+00	0.313	0.317
CCT3	-0.1054	1.00E+00	0.64	0.595
SLMAP	-0.1056	1.00E+00	0.292	0.295
BRIX1	-0.1057	1.00E+00	0.348	0.328
PDIA4	-0.1061	1.00E+00	0.507	0.476
HNRNPR	-0.1062	1.00E+00	0.477	0.463
MRPS2	-0.1062	1.00E+00	0.434	0.414
SHISA5	-0.1065	1.00E+00	0.534	0.483
STMN1	-0.1066	5.90E-01	0.611	0.612
TBRG4	-0.1066	1.00E+00	0.323	0.305
UBE2C	-0.1067	1.00E+00	0.555	0.567
TMC6	-0.1069	1.00E+00	0.251	0.254
GNAS	-0.1071	1.00E+00	0.507	0.465
RCC1	-0.1075	1.00E+00	0.344	0.328
IER5	-0.1078	2.20E-07	0.284	0.31
SPAG9	-0.1085	1.00E+00	0.481	0.44
RSL1D1	-0.1085	6.97E-01	0.653	0.627
MAPRE1	-0.1086	1.00E+00	0.47	0.426
MVP	-0.1086	1.00E+00	0.38	0.377
SLC39A3	-0.1088	9.94E-03	0.318	0.332
CLTC	-0.1088	1.00E+00	0.357	0.323
TRIM28	-0.1089	1.00E+00	0.378	0.345
SLC38A5	-0.1089	1.00E+00	0.33	0.329
SUZ12	-0.1091	1.00E+00	0.369	0.365
SGK1	-0.1092	1.00E+00	0.301	0.304
GRB2	-0.1093	7.90E-01	0.361	0.356
ROCK2	-0.1094	1.00E+00	0.319	0.29
LLGL2	-0.1094	1.00E+00	0.513	0.462
CLPTM1	-0.1095	1.00E+00	0.32	0.312
SLC25A39	-0.1095	5.87E-02	0.701	0.678
PPAN	-0.1099	1.87E-04	0.292	0.316
TPM4	-0.1101	3.66E-01	0.681	0.66
RASSF7	-0.1106	3.07E-01	0.382	0.389
RAD23B	-0.1109	1.00E+00	0.424	0.382
GATAD2A	-0.1110	1.00E+00	0.333	0.288
SEPT9	-0.1112	1.00E+00	0.433	0.401
RPL7L1	-0.1112	1.00E+00	0.408	0.375
CDK12	-0.1113	1.00E+00	0.367	0.355
B3GAT3	-0.1115	1.00E+00	0.334	0.34
STAU1	-0.1118	1.24E-01	0.539	0.519
SNRPA	-0.1119	1.00E+00	0.329	0.31
RAB7A	-0.1119	6.79E-03	0.653	0.623

SEPT2	-0.1121	1.00E+00	0.292	0.295
YDJC	-0.1122	1.00E+00	0.556	0.527
RCN1	-0.1123	1.00E+00	0.689	0.648
OTUB1	-0.1126	1.00E+00	0.414	0.404
SSBP4	-0.1126	1.00E+00	0.399	0.396
WDR18	-0.1128	2.07E-03	0.392	0.398
LDHA	-0.1130	2.62E-03	0.84	0.857
FAM83H	-0.1132	1.00E+00	0.264	0.239
C1QBP	-0.1133	7.83E-01	0.654	0.64
HES6	-0.1133	1.00E+00	0.25	0.25
TPGS1	-0.1135	3.32E-03	0.295	0.316
H2AFX	-0.1135	7.82E-01	0.332	0.335
GAR1	-0.1136	1.00E+00	0.376	0.378
NUDT15	-0.1137	1.00E+00	0.268	0.273
TPX2	-0.1139	1.00E+00	0.309	0.299
RAD21	-0.1139	1.00E+00	0.544	0.507
SMC1A	-0.1144	1.00E+00	0.317	0.299
HDLBP	-0.1144	1.00E+00	0.411	0.396
XRCC6	-0.1147	1.00E+00	0.553	0.512
SCAMP4	-0.1147	3.46E-04	0.258	0.277
EGR1	-0.1147	4.39E-01	0.573	0.573
FUS	-0.1149	3.36E-06	0.609	0.59
SSRP1	-0.1152	1.00E+00	0.475	0.458
IGF2BP2	-0.1155	1.00E+00	0.424	0.381
TUBG1	-0.1157	1.00E+00	0.343	0.333
KLK6	-0.1158	4.26E-01	0.771	0.789
SURF4	-0.1158	3.85E-02	0.384	0.389
NOLC1	-0.1159	1.00E+00	0.472	0.425
EHF	-0.1160	1.00E+00	0.544	0.516
PLIN3	-0.1164	1.00E+00	0.533	0.486
GOT2	-0.1165	1.00E+00	0.291	0.291
GTPBP4	-0.1168	1.00E+00	0.401	0.384
STK25	-0.1173	1.46E-06	0.271	0.3
FKBP8	-0.1173	3.64E-02	0.651	0.613
HSP90B1	-0.1174	1.28E-03	0.768	0.769
MDFI	-0.1176	1.17E-01	0.261	0.271
TUBB	-0.1177	2.17E-02	0.701	0.693
SLC1A5	-0.1178	1.00E+00	0.354	0.351
LSR	-0.1180	1.88E-01	0.623	0.586
A4GALT	-0.1180	1.00E+00	0.374	0.329
RPUSD1	-0.1186	1.90E-02	0.28	0.294
CCT7	-0.1188	1.00E+00	0.532	0.484
CGREF1	-0.1189	1.00E+00	0.274	0.266
WDR43	-0.1189	1.00E+00	0.452	0.424
TUFM	-0.1191	3.23E-02	0.647	0.619
ACOT7	-0.1194	1.00E+00	0.472	0.437
PES1	-0.1196	1.00E+00	0.25	0.234
HNRNPU	-0.1198	1.00E+00	0.524	0.496
CSE1L	-0.1201	1.00E+00	0.355	0.343
TUBA1C	-0.1202	3.14E-02	0.641	0.631
PSMB1	-0.1205	1.44E-08	0.742	0.752
CTSV	-0.1206	1.00E+00	0.348	0.341

CDV3	-0.1209	1.76E-02	0.661	0.632
DBNL	-0.1212	9.78E-01	0.399	0.388
GALNT1	-0.1213	1.00E+00	0.307	0.311
LINC00657	-0.1223	1.00E+00	0.394	0.357
DIRAS3	-0.1224	1.00E+00	0.355	0.349
ACTB	-0.1225	9.43E-18	0.918	0.935
IL20RA	-0.1226	1.00E+00	0.554	0.535
SIRT7	-0.1228	3.46E-01	0.314	0.32
SERTAD1	-0.1232	1.00E+00	0.353	0.345
H2AFZ	-0.1234	6.21E-05	0.732	0.751
CAPN1	-0.1236	1.00E+00	0.58	0.544
PLK2	-0.1236	1.00E+00	0.402	0.385
MT-CYB	-0.1237	1.01E-02	0.758	0.818
CORO1C	-0.1240	1.00E+00	0.271	0.272
MFSD12	-0.1240	1.00E+00	0.314	0.309
IMPDH1	-0.1244	4.33E-05	0.289	0.313
WDR34	-0.1245	1.00E+00	0.453	0.418
TGFB1	-0.1248	1.00E+00	0.525	0.496
PPP1CA	-0.1248	6.58E-02	0.682	0.655
EPCAM	-0.1249	3.55E-10	0.804	0.827
GADD45A	-0.1249	3.84E-31	0.473	0.516
C8orf82	-0.1250	5.19E-06	0.283	0.311
CCNB1	-0.1251	1.00E+00	0.31	0.313
SRSF2	-0.1252	4.35E-04	0.643	0.617
KDEL2	-0.1255	1.17E-01	0.659	0.633
PPFIBP1	-0.1256	1.00E+00	0.427	0.417
EI24	-0.1259	1.00E+00	0.558	0.521
POLDIP2	-0.1273	1.00E+00	0.433	0.409
WBP11	-0.1274	1.00E+00	0.431	0.407
NR2F6	-0.1275	4.49E-01	0.487	0.46
TMEM259	-0.1275	1.00E+00	0.322	0.313
TUBB2A	-0.1278	1.00E+00	0.478	0.451
ARRDC1	-0.1281	1.00E+00	0.511	0.485
KHDRBS1	-0.1282	1.00E+00	0.504	0.475
STMN3	-0.1284	1.00E+00	0.426	0.348
MARCKSL1	-0.1286	3.46E-01	0.591	0.569
POR	-0.1287	1.00E+00	0.3	0.301
COL6A1	-0.1291	3.28E-02	0.25	0.268
HDGF	-0.1292	9.82E-02	0.509	0.477
HNRNPD	-0.1301	1.00E+00	0.584	0.557
DDB1	-0.1302	1.00E+00	0.305	0.288
RUVBL2	-0.1304	1.00E+00	0.482	0.447
JUP	-0.1308	1.00E+00	0.584	0.556
HBEGF	-0.1314	1.00E+00	0.29	0.291
NELFB	-0.1317	1.00E+00	0.283	0.279
CCT6A	-0.1318	1.27E-02	0.665	0.645
BCLAF1	-0.1325	5.77E-01	0.426	0.417
EPRS	-0.1325	3.07E-04	0.342	0.365
EPHA2	-0.1328	1.00E+00	0.364	0.34
LRRC59	-0.1329	5.52E-04	0.652	0.625
RTN4	-0.1333	7.02E-09	0.747	0.737
SDC1	-0.1334	5.60E-10	0.372	0.395

THRAP3	-0.1336	1.00E+00	0.467	0.434
SLC7A5	-0.1338	1.00E+00	0.275	0.274
TUBB6	-0.1340	1.00E+00	0.316	0.311
HMGN2	-0.1342	1.46E-05	0.645	0.664
ITGA3	-0.1345	1.00E+00	0.395	0.368
HGS	-0.1347	1.00E+00	0.434	0.405
PDLIM7	-0.1349	5.58E-02	0.367	0.368
ANKRD11	-0.1356	1.00E+00	0.437	0.423
HSF1	-0.1363	1.00E+00	0.474	0.438
PHLDB2	-0.1367	1.76E-01	0.341	0.355
CAV1	-0.1367	2.73E-05	0.717	0.716
EIF4A3	-0.1372	1.00E+00	0.468	0.44
RHBDD2	-0.1372	1.37E-01	0.295	0.304
CSNK1D	-0.1374	1.14E-01	0.306	0.314
CCDC86	-0.1377	9.94E-03	0.283	0.298
PRSS22	-0.1377	8.36E-05	0.562	0.581
UBC	-0.1382	7.30E-32	0.847	0.859
SPTBN1	-0.1386	1.00E+00	0.477	0.445
NCL	-0.1389	9.07E-07	0.696	0.702
LGALS3BP	-0.1393	1.84E-06	0.64	0.613
SEMA3B	-0.1394	1.00E+00	0.428	0.419
VPS51	-0.1402	2.77E-06	0.269	0.294
DDX39A	-0.1403	2.89E-02	0.325	0.335
SF1	-0.1403	7.90E-07	0.484	0.482
ALYREF	-0.1404	1.10E-05	0.27	0.294
MAD1L1	-0.1408	2.62E-07	0.266	0.299
CDC37	-0.1408	2.53E-03	0.618	0.583
RBM42	-0.1409	1.00E+00	0.452	0.417
EIF3I	-0.1413	1.82E-05	0.655	0.632
ZFP36L2	-0.1414	1.00E+00	0.446	0.426
CENPF	-0.1417	1.00E+00	0.281	0.3
TSC22D1	-0.1422	3.48E-06	0.644	0.64
DNAJC21	-0.1422	1.00E+00	0.306	0.303
MISP	-0.1423	6.16E-01	0.435	0.416
TOMM40	-0.1425	5.04E-01	0.515	0.489
CYP2W1	-0.1425	1.00E+00	0.294	0.294
ARF1	-0.1430	1.64E-13	0.709	0.69
RRP1	-0.1432	1.00E+00	0.32	0.312
VPS37B	-0.1433	4.55E-01	0.251	0.257
MCM7	-0.1435	1.00E+00	0.354	0.347
DST	-0.1441	1.00E+00	0.394	0.378
TK1	-0.1442	1.00E+00	0.452	0.45
KLF5	-0.1443	1.00E+00	0.301	0.305
CHPF	-0.1447	6.50E-01	0.389	0.388
BCL2L1	-0.1448	2.02E-06	0.583	0.581
SLC52A2	-0.1448	2.41E-04	0.465	0.453
DDX54	-0.1448	7.22E-04	0.302	0.313
MLF2	-0.1449	1.45E-06	0.651	0.632
BSG	-0.1451	2.11E-15	0.766	0.768
PSMD2	-0.1453	1.00E+00	0.486	0.461
EPS8L2	-0.1453	3.58E-02	0.412	0.405
LRRC61	-0.1454	1.00E+00	0.37	0.361

ST14	-0.1456	1.00E+00	0.496	0.46
RRBP1	-0.1456	1.00E+00	0.579	0.551
SPINT1	-0.1458	2.88E-01	0.545	0.52
SH3GLB2	-0.1461	1.14E-03	0.375	0.38
BPTF	-0.1464	7.49E-05	0.301	0.319
NOC2L	-0.1464	6.52E-01	0.337	0.332
HNRNPA0	-0.1467	1.41E-06	0.448	0.448
PDIA3	-0.1468	3.68E-02	0.685	0.647
DUSP1	-0.1469	1.30E-03	0.339	0.361
ITGA6	-0.1472	1.00E+00	0.352	0.353
VCP	-0.1472	1.00E+00	0.458	0.429
FAM84B	-0.1475	4.63E-03	0.279	0.293
AMN	-0.1487	1.65E-01	0.439	0.435
CCT5	-0.1498	1.00E+00	0.586	0.549
EFNB2	-0.1498	8.02E-03	0.31	0.318
RNH1	-0.1507	2.97E-03	0.636	0.596
YBX1	-0.1507	7.67E-24	0.875	0.895
LRRC8A	-0.1514	1.00E+00	0.31	0.294
THEM6	-0.1516	2.10E-04	0.399	0.401
PTPN12	-0.1517	1.00E+00	0.489	0.463
BAIAP2	-0.1520	1.00E+00	0.518	0.483
LIF	-0.1521	1.00E+00	0.257	0.269
MMP7	-0.1522	1.06E-09	0.696	0.728
SNX9	-0.1526	4.56E-05	0.34	0.357
SFPQ	-0.1529	1.00E+00	0.47	0.44
HPCAL1	-0.1534	9.08E-01	0.487	0.463
LY6D	-0.1535	1.21E-03	0.568	0.594
PUF60	-0.1538	1.00E+00	0.547	0.514
NAE1	-0.1541	4.30E-06	0.346	0.375
SAPCD2	-0.1544	1.28E-04	0.269	0.29
KRT18	-0.1546	1.42E-19	0.943	0.97
MROH6	-0.1547	2.16E-01	0.301	0.314
SNRPB	-0.1552	5.40E-07	0.695	0.697
PRKCDBP	-0.1553	1.00E+00	0.409	0.401
REPIN1	-0.1563	4.22E-06	0.306	0.323
EREG	-0.1565	1.63E-05	0.494	0.496
NES	-0.1567	1.00E+00	0.302	0.278
CDC42EP1	-0.1567	5.26E-04	0.502	0.489
PTRF	-0.1577	7.75E-03	0.381	0.385
TIMP3	-0.1577	1.00E+00	0.313	0.317
NCLN	-0.1580	4.04E-03	0.338	0.338
SMARCA4	-0.1583	4.66E-05	0.431	0.426
SYNCRIP	-0.1590	9.21E-03	0.591	0.571
UNC93B1	-0.1591	4.65E-04	0.35	0.355
SYNE2	-0.1593	1.00E+00	0.358	0.365
FOS	-0.1600	8.23E-06	0.64	0.64
SLC2A1	-0.1629	5.30E-10	0.7	0.693
GNG4	-0.1639	6.86E-04	0.467	0.459
EIF4H	-0.1647	4.71E-09	0.565	0.551
PVRL2	-0.1669	1.33E-06	0.376	0.387
LRRFIP1	-0.1672	5.12E-06	0.525	0.522
TM4SF1	-0.1677	5.93E-26	0.771	0.79

FBXW5	-0.1677	1.58E-05	0.385	0.391
SERPINB5	-0.1682	4.02E-04	0.294	0.317
KRT20	-0.1692	6.44E-04	0.659	0.661
TCEB3	-0.1694	5.19E-03	0.304	0.317
EHD1	-0.1706	1.78E-02	0.365	0.354
DUS1L	-0.1712	1.79E-05	0.454	0.441
TUBA1B	-0.1716	6.89E-06	0.684	0.693
ILF3	-0.1753	1.27E-01	0.468	0.448
PODXL2	-0.1754	1.43E-06	0.423	0.426
ANLN	-0.1767	4.57E-03	0.291	0.31
ARL4C	-0.1777	3.71E-05	0.38	0.39
CDC20	-0.1778	2.46E-03	0.339	0.361
PLEC	-0.1780	1.00E+00	0.501	0.456
DUSP5	-0.1790	3.49E-09	0.361	0.391
EIF4G1	-0.1798	5.79E-02	0.511	0.484
ACTG1	-0.1811	6.97E-32	0.891	0.914
P4HB	-0.1813	4.45E-18	0.738	0.73
EEF2	-0.1845	1.86E-22	0.816	0.831
PKN1	-0.1850	1.05E-11	0.327	0.355
PLAUR	-0.1853	3.69E-10	0.51	0.52
RAB8A	-0.1858	4.19E-07	0.353	0.362
ACTN4	-0.1858	1.41E-14	0.696	0.683
SLC20A1	-0.1873	1.00E+00	0.341	0.329
ETS2	-0.1875	3.30E-04	0.301	0.315
PKP3	-0.1907	1.46E-07	0.526	0.504
MGAT4B	-0.1907	4.72E-19	0.278	0.321
ADAP1	-0.1913	4.67E-15	0.419	0.451
ENO1	-0.1937	3.44E-11	0.776	0.777
ENC1	-0.1945	7.81E-12	0.267	0.308
MALL	-0.1947	1.06E-08	0.516	0.523
LAD1	-0.1952	2.92E-07	0.533	0.516
MT-CO3	-0.1958	8.99E-14	0.778	0.849
KRT8	-0.1965	9.60E-33	0.94	0.969
TINAGL1	-0.1983	2.09E-10	0.541	0.527
GIPC1	-0.2001	2.26E-06	0.59	0.555
RNF187	-0.2001	1.62E-11	0.298	0.321
URI1	-0.2007	1.90E-09	0.369	0.378
KLF3	-0.2013	4.70E-02	0.314	0.318
MT-ND4L	-0.2016	6.93E-09	0.564	0.583
UBALD2	-0.2020	8.97E-18	0.543	0.567
TRAP1	-0.2028	2.44E-05	0.429	0.421
PPP1R14B	-0.2036	1.29E-22	0.695	0.703
KRT23	-0.2047	1.00E+00	0.331	0.349
GJB3	-0.2066	7.26E-07	0.361	0.364
GPRC5A	-0.2079	1.17E-31	0.758	0.799
PTBP1	-0.2079	1.22E-17	0.427	0.449
SLC16A3	-0.2087	4.03E-09	0.642	0.617
UBE2S	-0.2094	3.72E-07	0.571	0.582
UBE2M	-0.2095	2.34E-11	0.437	0.442
COTL1	-0.2112	6.67E-13	0.509	0.518
PKM	-0.2126	5.67E-16	0.769	0.775
PIM3	-0.2182	2.68E-11	0.33	0.35

MIDN	-0.2189	1.51E-06	0.428	0.434
CCND1	-0.2192	1.87E-16	0.738	0.756
SOX9	-0.2284	1.30E-03	0.478	0.466
CKB	-0.2284	7.01E-13	0.629	0.645
BOP1	-0.2300	1.43E-12	0.455	0.46
CITED4	-0.2363	1.27E-09	0.394	0.393
EIF3B	-0.2367	5.07E-09	0.435	0.429
TRIB1	-0.2401	6.84E-17	0.302	0.344
EDN1	-0.2420	6.46E-03	0.393	0.404
ARHGDIA	-0.2449	1.44E-28	0.679	0.675
GDF15	-0.2464	1.24E-03	0.374	0.395
PHLDA2	-0.2469	4.96E-49	0.776	0.799
TUBB4B	-0.2475	5.87E-21	0.735	0.753
ZFP36	-0.2497	2.94E-12	0.424	0.458
LAMA3	-0.2511	3.90E-08	0.429	0.437
PLAU	-0.2516	1.87E-06	0.416	0.426
CLDN3	-0.2558	4.27E-33	0.729	0.763
RHOB	-0.2597	7.74E-31	0.713	0.726
ADM	-0.2624	1.23E-21	0.538	0.565
DUSP2	-0.2624	4.43E-42	0.251	0.331
IGFBP3	-0.2626	8.44E-04	0.5	0.494
LAMB3	-0.2639	3.32E-18	0.496	0.515
TACSTD2	-0.2694	2.91E-38	0.731	0.758
MKI67	-0.2720	6.32E-05	0.35	0.369
DUSP6	-0.2777	9.87E-13	0.535	0.534
EZR	-0.2834	7.04E-51	0.801	0.834
FOSL1	-0.2843	2.70E-30	0.472	0.514
JUNB	-0.2846	1.36E-39	0.688	0.704
DSP	-0.2905	1.74E-15	0.577	0.574
SOCS3	-0.2912	1.06E-27	0.362	0.404
ELF3	-0.3164	3.30E-62	0.724	0.756
AKAP12	-0.3350	1.57E-35	0.775	0.816
KLF10	-0.3721	3.10E-67	0.306	0.407
VWA1	-0.3886	3.62E-31	0.443	0.461
SFN	-0.4019	1.78E-61	0.719	0.763
KRT17	-0.4020	6.58E-31	0.565	0.603
EMP1	-0.4103	6.35E-82	0.661	0.699
IER2	-0.4245	8.67E-107	0.726	0.753
CLDN4	-0.4276	1.24E-132	0.777	0.839
LMNA	-0.4549	6.23E-130	0.741	0.786
IGFBP2	-0.4782	6.08E-38	0.326	0.378
IER3	-0.5982	3.70E-193	0.768	0.825
ID1	-0.6150	5.83E-92	0.573	0.649
HES1	-0.9168	0.00E+00	0.537	0.687

Supplementary Table 3. List of top 50 representative genes for each epithelial sub-cluster.

cluster	gene	log2_avgFC	p_val_adj	pct.1	pct.2
Epi_1	C6orf15	1.2641	0.00E+00	0.821	0.547
Epi_1	LCN2	1.2500	0.00E+00	0.983	0.727
Epi_1	KRT17	1.0443	0.00E+00	0.891	0.524
Epi_1	KLK6	0.9623	0.00E+00	0.974	0.741
Epi_1	PRSS22	0.8683	0.00E+00	0.847	0.515
Epi_1	TIMP3	0.8482	0.00E+00	0.59	0.256
Epi_1	KRT5	0.8249	0.00E+00	0.373	0.094
Epi_1	S100A4	0.8012	0.00E+00	0.966	0.811
Epi_1	CFD	0.7529	0.00E+00	0.841	0.533
Epi_1	BST2	0.7118	0.00E+00	0.773	0.378
Epi_1	KLK5	0.7010	0.00E+00	0.494	0.188
Epi_1	IL20RA	0.6846	0.00E+00	0.79	0.487
Epi_1	TMSB4X	0.6842	0.00E+00	0.999	0.958
Epi_1	RNASE1	0.6524	0.00E+00	0.447	0.141
Epi_1	GSN	0.6253	0.00E+00	0.8	0.478
Epi_1	C9orf16	0.6102	0.00E+00	0.969	0.739
Epi_1	KRT19	0.6032	0.00E+00	0.998	0.917
Epi_1	CD9	0.5853	0.00E+00	0.988	0.818
Epi_1	RABAC1	0.5833	0.00E+00	0.803	0.497
Epi_1	LEMD1	0.5755	0.00E+00	0.45	0.101
Epi_1	RPL3	0.5165	0.00E+00	0.995	0.918
Epi_1	EEF1A1	0.5128	0.00E+00	0.998	0.961
Epi_1	RPL10	0.5082	0.00E+00	0.998	0.952
Epi_1	CD24	0.6908	4.23E-299	0.909	0.638
Epi_1	CD63	0.5459	3.68E-298	0.962	0.741
Epi_1	S100A2	0.9454	4.96E-295	0.707	0.391
Epi_1	RARRES3	1.2046	3.66E-293	0.719	0.386
Epi_1	SERPINA1	0.9389	7.23E-289	0.554	0.241
Epi_1	GLIPR1	0.6308	6.17E-286	0.549	0.236
Epi_1	CST6	0.8692	4.22E-276	0.807	0.536
Epi_1	SAT1	0.7140	1.01E-275	0.964	0.745
Epi_1	TSPAN1	0.5907	2.44E-273	0.87	0.584
Epi_1	CYP2W1	0.7050	1.59E-252	0.537	0.241
Epi_1	SOX4	0.6315	4.95E-236	0.72	0.415
Epi_1	CLIC3	0.7429	1.24E-230	0.757	0.469
Epi_1	KLK7	0.5294	2.30E-227	0.735	0.431
Epi_1	PLA2G16	0.5130	9.17E-219	0.943	0.728
Epi_1	KLK1	0.5383	1.99E-217	0.402	0.157

cluster	gene	log2_avgFC	p_val_adj	pct.1	pct.2
Epi_1	RHOB	0.5039	6.27E-213	0.93	0.676
Epi_1	CTSV	0.5946	1.17E-203	0.558	0.296
Epi_1	PLAU	0.5713	5.85E-203	0.655	0.371
Epi_1	ID1	0.6527	5.45E-196	0.842	0.575
Epi_1	CTSD	0.5775	1.27E-188	0.896	0.691
Epi_1	CTSB	0.5100	7.92E-183	0.903	0.677
Epi_1	F3	0.5083	3.89E-154	0.771	0.519
Epi_1	AKAP12	0.6573	2.41E-145	0.922	0.776
Epi_1	ZFP36	0.5392	1.26E-136	0.635	0.405
Epi_1	MMP7	0.6442	2.93E-124	0.861	0.686
Epi_1	C15orf48	0.6516	6.25E-98	0.616	0.406
Epi_1	SPRR3	0.5891	4.01E-52	0.258	0.145
Epi_2	HIST1H4C	1.4444	0.00E+00	0.868	0.495
Epi_2	UBE2S	1.2225	0.00E+00	0.957	0.501
Epi_2	TUBA1B	1.0095	0.00E+00	0.982	0.63
Epi_2	H2AFV	0.9465	0.00E+00	0.929	0.44
Epi_2	PTTG1	0.9370	0.00E+00	0.877	0.379
Epi_2	H2AFZ	0.9234	0.00E+00	0.998	0.693
Epi_2	MKI67	0.9032	0.00E+00	0.81	0.271
Epi_2	RRM2	0.8931	0.00E+00	0.748	0.237
Epi_2	TUBB4B	0.8522	0.00E+00	0.971	0.701
Epi_2	CDKN3	0.8360	0.00E+00	0.807	0.289
Epi_2	RANBP1	0.8334	0.00E+00	0.98	0.626
Epi_2	DIRAS3	0.8321	0.00E+00	0.691	0.282
Epi_2	STMN1	0.7918	0.00E+00	0.948	0.542
Epi_2	HMGN2	0.7788	0.00E+00	0.984	0.59
Epi_2	CAV1	0.7708	0.00E+00	0.979	0.662
Epi_2	HMGB2	0.7680	0.00E+00	0.847	0.371
Epi_2	CCNB1	0.7601	0.00E+00	0.656	0.241
Epi_2	CENPW	0.7521	0.00E+00	0.881	0.378
Epi_2	SET	0.7346	0.00E+00	0.983	0.666
Epi_2	GAL	0.7126	0.00E+00	0.852	0.45
Epi_2	KIAA0101	0.7090	0.00E+00	0.7	0.232
Epi_2	SLC25A5	0.7078	0.00E+00	0.979	0.639
Epi_2	WDR34	0.6909	0.00E+00	0.781	0.357
Epi_2	TK1	0.6793	0.00E+00	0.83	0.372
Epi_2	PGAM1	0.6720	0.00E+00	0.937	0.571
Epi_2	DTYMK	0.6544	0.00E+00	0.748	0.301
Epi_2	NUCKS1	0.6503	0.00E+00	0.911	0.466
Epi_2	DUT	0.6329	0.00E+00	0.864	0.471
Epi_2	LDHB	0.6254	0.00E+00	0.991	0.712
Epi_2	PPP1R14B	0.6247	0.00E+00	0.957	0.648
Epi_2	ATP5G3	0.6183	0.00E+00	0.969	0.638
Epi_2	BIRC5	0.6113	0.00E+00	0.79	0.294
Epi_2	HMGB1	0.6068	0.00E+00	0.998	0.749
Epi_2	RAN	0.5988	0.00E+00	0.992	0.73
Epi_2	CCNB2	0.5913	0.00E+00	0.548	0.195
Epi_2	MZT2B	0.5880	0.00E+00	0.956	0.645
Epi_2	RHOBTB3	0.5843	0.00E+00	0.754	0.347
Epi_2	DNAJC9	0.5830	0.00E+00	0.763	0.341

cluster	gene	log2_avgFC	p_val_adj	pct.1	pct.2
Epi_2	CENPF	0.5770	0.00E+00	0.633	0.224
Epi_2	PHF19	0.5749	0.00E+00	0.592	0.184
Epi_2	CDC20	0.5748	0.00E+00	0.686	0.285
Epi_2	POLR2F	0.5695	0.00E+00	0.943	0.607
Epi_2	SNRPG	0.5617	0.00E+00	0.935	0.57
Epi_2	PRDX2	0.5586	0.00E+00	0.969	0.65
Epi_2	NDUFB2	0.5553	3.42E-302	0.982	0.705
Epi_2	TUBB	0.5947	5.10E-302	0.95	0.644
Epi_2	UBE2C	0.7721	7.22E-297	0.885	0.497
Epi_2	ENO1	0.5656	1.81E-290	0.989	0.733
Epi_2	IGFBP2	0.6022	2.44E-279	0.654	0.3
Epi_2	LGALS1	0.5795	4.01E-196	0.961	0.71
Epi_3	PTMA	0.5847	1.21E-189	0.931	0.961
Epi_3	HSP90AB1	0.7277	8.38E-103	0.745	0.91
Epi_3	HSP90AA1	0.6337	7.40E-94	0.77	0.899
Epi_3	RPL21	0.5809	9.40E-75	0.749	0.907
Epi_3	MORF4L1	0.4815	8.08E-45	0.272	0.588
Epi_3	PSMC5	0.4889	7.83E-44	0.287	0.618
Epi_3	SUMO1	0.5194	3.40E-42	0.284	0.605
Epi_3	HNRNPU	0.4822	4.74E-41	0.252	0.543
Epi_3	PSMA3	0.5022	4.83E-41	0.294	0.626
Epi_3	AIMP1	0.5468	4.93E-39	0.267	0.564
Epi_3	RAD21	0.5155	1.56E-35	0.272	0.556
Epi_3	HNRNPK	0.4889	1.70E-31	0.318	0.647
Epi_3	STIP1	0.4810	2.54E-31	0.271	0.543
Epi_3	SH3KBP1	0.6036	4.41E-30	0.271	0.544
Epi_3	CCT5	0.5364	5.37E-30	0.3	0.6
Epi_3	TPM3	0.5088	1.06E-29	0.337	0.679
Epi_3	GDI2	0.4938	2.39E-29	0.312	0.625
Epi_3	CALM2	0.5292	4.46E-29	0.659	0.899
Epi_3	ATP5A1	0.4959	1.85E-28	0.287	0.569
Epi_3	SRRM1	0.5137	6.18E-27	0.335	0.659
Epi_3	GLO1	0.6034	9.91E-27	0.301	0.594
Epi_3	CAPZA2	0.6529	2.78E-26	0.252	0.501
Epi_3	COTL1	0.5509	7.17E-25	0.286	0.549
Epi_3	BZW1	0.6663	1.51E-23	0.261	0.507
Epi_3	EIF5B	0.5616	3.46E-23	0.346	0.673
Epi_3	SNRPB2	0.5071	1.95E-22	0.33	0.634
Epi_3	LSM3	0.5470	7.67E-21	0.326	0.629
Epi_3	HMGB1	0.6781	2.67E-20	0.607	0.819
Epi_3	SSB	0.6696	8.19E-20	0.314	0.601
Epi_3	RSL24D1	0.6251	3.23E-17	0.322	0.607
Epi_3	PDAP1	0.5649	1.96E-16	0.357	0.676
Epi_3	CCT8	0.5924	1.20E-14	0.327	0.6
Epi_3	KPNA2	0.6106	1.57E-14	0.256	0.453
Epi_3	TMED2	0.6810	3.54E-14	0.335	0.616
Epi_3	HNRNPC	0.5210	4.99E-12	0.386	0.717
Epi_3	TAX1BP1	0.6379	2.57E-09	0.382	0.685
Epi_3	SNRPD2	0.5624	1.64E-08	0.414	0.77
Epi_3	EIF3E	0.9271	1.51E-07	0.527	0.782
Epi_3	TKT	0.5191	1.72E-07	0.412	0.738

cluster	gene	log2_avgFC	p_val_adj	pct.1	pct.2
Epi_3	NNMT	0.5931	4.39E-07	0.279	0.457
Epi_3	VDAC1	0.5162	4.32E-06	0.412	0.738
Epi_3	PSMA4	0.8497	2.42E-02	0.35	0.59
Epi_3	HMGB2	0.5902	1.00E+00	0.333	0.47
Epi_3	TMEM123	0.5288	1.00E+00	0.535	0.849
Epi_3	HMG2	0.5458	1.00E+00	0.438	0.69
Epi_3	SEPT7	0.9121	1.00E+00	0.385	0.614
Epi_3	PTGES3	0.7229	1.00E+00	0.493	0.777
Epi_3	YWHAQ	0.5618	1.00E+00	0.464	0.755
Epi_3	UBE2C	0.5276	1.00E+00	0.417	0.585
Epi_3	NCL	0.7180	1.00E+00	0.461	0.735
Epi_4	TUBA1B	0.9153	0.00E+00	0.983	0.649
Epi_4	CCNB1	0.9062	0.00E+00	0.707	0.257
Epi_4	PSMA7	0.8744	0.00E+00	0.995	0.714
Epi_4	CYC1	0.8509	0.00E+00	0.981	0.622
Epi_4	C1QBP	0.8426	0.00E+00	0.96	0.602
Epi_4	SNRBP	0.8245	0.00E+00	0.986	0.656
Epi_4	EIF5A	0.7749	0.00E+00	0.984	0.642
Epi_4	LYZ	0.7597	0.00E+00	0.872	0.431
Epi_4	FABP5	0.7566	0.00E+00	0.965	0.571
Epi_4	PCNA	0.7292	0.00E+00	0.767	0.291
Epi_4	CTNNA1	0.7189	0.00E+00	0.867	0.405
Epi_4	HMGB2	0.7100	0.00E+00	0.883	0.393
Epi_4	MAL2	0.7030	0.00E+00	0.979	0.642
Epi_4	ATP5A1	0.7010	0.00E+00	0.903	0.481
Epi_4	CDC20	0.6980	0.00E+00	0.747	0.299
Epi_4	AURKA	0.6927	0.00E+00	0.561	0.143
Epi_4	MRPS26	0.6830	0.00E+00	0.88	0.464
Epi_4	BIRC5	0.6732	0.00E+00	0.826	0.317
Epi_4	COPRS	0.6730	0.00E+00	0.892	0.48
Epi_4	FKBP1A	0.6687	0.00E+00	0.965	0.625
Epi_4	ATP5G1	0.6631	0.00E+00	0.951	0.58
Epi_4	PFN1	0.6590	0.00E+00	0.996	0.766
Epi_4	NME1	0.6438	0.00E+00	0.993	0.703
Epi_4	TMEM14B	0.6305	0.00E+00	0.911	0.509
Epi_4	TXNL4A	0.6258	0.00E+00	0.878	0.453
Epi_4	GCSH	0.6239	0.00E+00	0.813	0.364
Epi_4	CACYBP	0.6149	0.00E+00	0.93	0.527
Epi_4	COX5A	0.5930	0.00E+00	0.978	0.654
Epi_4	NDUFB9	0.5850	1.43E-303	0.994	0.718
Epi_4	UBE2S	0.7675	1.44E-301	0.945	0.528
Epi_4	LAPTM4B	0.5780	5.14E-300	0.789	0.376
Epi_4	YWHAQ	0.6157	6.10E-300	0.981	0.681
Epi_4	PA2G4	0.5971	4.90E-299	0.972	0.621
Epi_4	KPNA2	0.6326	6.30E-297	0.81	0.375
Epi_4	PSMB6	0.6038	6.99E-297	0.937	0.583
Epi_4	RAN	0.6076	2.35E-296	0.995	0.745
Epi_4	CKS1B	0.6180	2.58E-294	0.914	0.484
Epi_4	CKS2	0.6872	1.29E-291	0.852	0.425
Epi_4	DNPH1	0.5951	1.76E-276	0.927	0.553
Epi_4	H2AFZ	0.6560	2.15E-274	0.995	0.71

cluster	gene	log2_avgFC	p_val_adj	pct.1	pct.2
Epi_4	HMG2	0.6253	9.06E-262	0.972	0.614
Epi_4	LDHB	0.5961	6.68E-250	0.994	0.727
Epi_4	PTTG1	0.5904	2.49E-248	0.855	0.41
Epi_4	MT1E	0.6558	1.76E-237	0.886	0.484
Epi_4	HIST1H4C	0.9081	8.88E-227	0.881	0.514
Epi_4	ENO1	0.6012	4.10E-219	0.993	0.747
Epi_4	UBE2C	0.8353	4.00E-217	0.883	0.519
Epi_4	MT2A	0.7232	1.73E-212	0.845	0.475
Epi_4	SLIRP	0.6271	8.94E-198	0.962	0.63
Epi_4	CKB	0.6556	1.02E-178	0.926	0.6
Epi_5	MALAT1	2.9357	0.00E+00	0.968	0.895
Epi_5	MT-ND2	1.7027	0.00E+00	0.903	0.846
Epi_5	MT-CO1	1.1799	1.44E-224	0.874	0.839
Epi_5	NEAT1	2.6064	1.09E-221	0.749	0.687
Epi_5	MT-ATP6	1.2772	2.43E-217	0.819	0.795
Epi_5	MT-ND1	1.2042	4.64E-212	0.846	0.842
Epi_5	MT-ND4	1.1277	1.55E-182	0.839	0.827
Epi_5	MT-ND5	1.3077	1.04E-147	0.747	0.791
Epi_5	MT-ND3	1.6868	9.52E-147	0.754	0.75
Epi_5	MT-CO3	1.0338	1.42E-117	0.835	0.823
Epi_5	MT-CYB	0.9495	7.07E-108	0.792	0.799
Epi_5	MT-CO2	0.8451	3.58E-104	0.83	0.804
Epi_5	XIST	1.7293	1.62E-96	0.463	0.331
Epi_5	MT-ND4L	1.3707	1.13E-54	0.554	0.579
Epi_5	SAT1	1.1190	1.64E-27	0.65	0.8
Epi_5	CCNL1	1.3398	3.32E-26	0.486	0.534
Epi_5	ELF3	1.0475	7.64E-26	0.598	0.763
Epi_5	GPRC5A	0.7711	5.10E-16	0.616	0.806
Epi_5	WSB1	1.0866	2.54E-14	0.274	0.228
Epi_5	SLC20A1	1.1907	4.11E-13	0.345	0.332
Epi_5	PLEC	1.1054	1.28E-11	0.419	0.478
Epi_5	N4BP2L2	1.0857	8.23E-10	0.284	0.258
Epi_5	ZNF292	1.0195	1.75E-08	0.27	0.243
Epi_5	JUND	1.1958	7.62E-08	0.362	0.382
Epi_5	KLF6	0.8623	8.24E-08	0.589	0.774
Epi_5	DST	0.9934	6.13E-07	0.36	0.386
Epi_5	LAMB3	1.0482	8.89E-07	0.432	0.518
Epi_5	LIF	0.9487	5.44E-06	0.279	0.263
Epi_5	LIPH	1.0827	1.47E-05	0.327	0.333
Epi_5	VMP1	1.2966	7.24E-05	0.41	0.496
Epi_5	POLR2J3	1.0337	1.36E-04	0.332	0.357
Epi_5	MIDN	1.0322	4.11E-04	0.383	0.438
Epi_5	SEMA3B	0.9849	1.08E-02	0.371	0.428
Epi_5	IFRD1	0.9275	1.23E-02	0.298	0.309
Epi_5	SLC38A2	0.9601	6.22E-02	0.32	0.35
Epi_5	PADI1	0.8720	9.18E-01	0.265	0.276
Epi_5	LAMA3	0.9011	1.00E+00	0.361	0.443
Epi_5	AKAP9	0.9115	1.00E+00	0.298	0.339
Epi_5	LMO7	0.8523	1.00E+00	0.345	0.41
Epi_5	SF1	0.9011	1.00E+00	0.382	0.494
Epi_5	SLC25A37	0.8320	1.00E+00	0.26	0.293

cluster	gene	log2_avgFC	p_val_adj	pct.1	pct.2
Epi_5	FUS	0.8543	1.00E+00	0.436	0.615
Epi_5	NPEPPS	0.8834	1.00E+00	0.313	0.384
Epi_5	PNISR	0.7934	1.00E+00	0.321	0.394
Epi_5	JUN	1.0376	1.00E+00	0.438	0.604
Epi_5	MACF1	0.7709	1.00E+00	0.295	0.371
Epi_5	FOSB	1.0348	1.00E+00	0.304	0.386
Epi_5	RNF213	0.8072	1.00E+00	0.292	0.364
Epi_5	ANKRD11	0.7997	1.00E+00	0.325	0.44
Epi_5	NAMPT	0.8524	1.00E+00	0.375	0.514
Epi_6	HSPA6	3.1143	0.00E+00	0.384	0.046
Epi_6	ZFAND2A	1.9023	0.00E+00	0.635	0.187
Epi_6	HSPB1	1.3175	9.52E-207	0.952	0.847
Epi_6	HERPUD1	1.0201	3.38E-203	0.559	0.225
Epi_6	DNAJB1	2.0658	1.44E-199	0.773	0.518
Epi_6	FTL	0.8417	7.76E-188	0.977	0.939
Epi_6	DNAJB9	0.6720	1.17E-184	0.401	0.123
Epi_6	BAG3	1.3564	2.76E-173	0.489	0.192
Epi_6	HSPA5	1.3696	7.15E-171	0.789	0.576
Epi_6	EIF1	0.5724	3.57E-170	0.965	0.895
Epi_6	HSPH1	1.4453	3.32E-162	0.671	0.388
Epi_6	HSPA1A	2.6801	1.34E-154	0.562	0.297
Epi_6	ZFAS1	0.9686	8.82E-154	0.882	0.691
Epi_6	SERP1	0.8338	2.40E-148	0.811	0.676
Epi_6	CRYAB	1.1485	6.38E-146	0.357	0.113
Epi_6	OSER1	0.7943	5.21E-123	0.523	0.258
Epi_6	DDIT3	0.6734	3.58E-116	0.39	0.146
Epi_6	OAZ1	0.6434	2.23E-113	0.937	0.824
Epi_6	SDF2L1	1.0734	1.40E-112	0.69	0.514
Epi_6	C6orf48	0.9322	1.42E-112	0.694	0.455
Epi_6	DNAJC3	0.5480	3.52E-112	0.459	0.206
Epi_6	HSPA1B	2.7510	1.37E-110	0.57	0.37
Epi_6	DEDD2	0.7856	1.94E-104	0.476	0.235
Epi_6	AGR2	0.7003	5.92E-103	0.333	0.127
Epi_6	SELK	0.7634	2.05E-100	0.675	0.485
Epi_6	VIMP	0.6587	5.56E-100	0.686	0.485
Epi_6	SERPINH1	1.1626	1.48E-99	0.541	0.314
Epi_6	CDK2AP2	0.6454	5.68E-84	0.575	0.379
Epi_6	SNHG7	0.7708	1.73E-83	0.654	0.456
Epi_6	TAF1D	0.6643	5.23E-83	0.709	0.517
Epi_6	EIF4A2	0.5590	3.91E-81	0.806	0.652
Epi_6	DNAJB11	0.5866	9.86E-76	0.553	0.368
Epi_6	DNAJA4	0.5699	2.62E-75	0.283	0.112
Epi_6	FKBP4	0.8433	3.41E-75	0.743	0.591
Epi_6	TAF7	0.8328	6.91E-71	0.624	0.429
Epi_6	PPP1R15A	0.9352	4.99E-67	0.707	0.519
Epi_6	KRT10	0.6335	2.33E-63	0.768	0.638
Epi_6	SAR1A	0.5848	2.36E-62	0.575	0.399
Epi_6	MANF	0.8589	6.60E-62	0.663	0.559
Epi_6	CACYBP	0.7197	5.02E-57	0.705	0.565
Epi_6	MT1X	0.7263	3.24E-56	0.347	0.176
Epi_6	MRPL18	0.8185	8.14E-50	0.67	0.547

cluster	gene	log2_avgFC	p_val_adj	pct.1	pct.2
Epi_6	YTHDF2	0.5722	2.94E-48	0.534	0.371
Epi_6	DNAJA1	0.7744	7.07E-36	0.577	0.467
Epi_6	PDIA4	0.5854	1.26E-31	0.564	0.48
Epi_6	HSPA8	0.6141	4.69E-27	0.803	0.702
Epi_6	STIP1	0.6534	7.06E-27	0.606	0.5
Epi_6	NUDC	0.6037	5.45E-24	0.764	0.689
Epi_6	SNRPB2	0.5517	1.42E-19	0.683	0.587
Epi_6	UBB	0.7628	9.20E-16	0.856	0.807
Epi_7	MT-CYB	1.4423	0.00E+00	0.994	0.782
Epi_7	MT-CO2	1.4228	0.00E+00	0.995	0.791
Epi_7	MT-CO3	1.3899	0.00E+00	0.998	0.81
Epi_7	MT-CO1	1.3789	0.00E+00	0.996	0.83
Epi_7	MT-ATP6	1.3520	0.00E+00	0.996	0.781
Epi_7	MT-ND4	1.3413	0.00E+00	0.998	0.814
Epi_7	MT-ND5	1.2718	0.00E+00	0.986	0.769
Epi_7	MT-ND1	1.2107	0.00E+00	0.999	0.829
Epi_7	MT-ND2	1.1164	0.00E+00	0.999	0.84
Epi_7	MT-ND3	1.0046	2.66E-186	0.978	0.732
Epi_7	MT-ND4L	0.8060	7.86E-167	0.813	0.557
Epi_7	CSTB	0.8011	3.28E-133	0.988	0.897
Epi_7	S100A11	0.5107	2.10E-128	0.998	0.948
Epi_7	ELF3	0.6695	7.59E-110	0.891	0.733
Epi_7	NEAT1	0.7480	2.91E-104	0.882	0.678
Epi_7	MALAT1	0.4484	1.33E-102	0.988	0.895
Epi_7	RPLP2	0.3748	3.44E-89	0.995	0.956
Epi_7	COX6B1	0.4539	2.45E-86	0.909	0.793
Epi_7	COX5B	0.3940	1.60E-81	0.946	0.826
Epi_7	S100A6	0.4450	7.99E-79	0.997	0.967
Epi_7	ADIRF	0.6323	3.15E-73	0.965	0.843
Epi_7	GPRC5A	0.5838	5.83E-69	0.912	0.775
Epi_7	TMA7	0.4979	2.76E-63	0.895	0.796
Epi_7	TXN	0.4193	5.79E-63	0.958	0.831
Epi_7	POLR2J3	0.4354	2.04E-62	0.522	0.341
Epi_7	CST3	0.4259	3.37E-62	0.928	0.817
Epi_7	FAM83H	0.4152	9.79E-62	0.417	0.234
Epi_7	PLEC	0.5080	3.08E-60	0.617	0.459
Epi_7	RRBP1	0.5775	2.11E-59	0.674	0.551
Epi_7	TMSB10	0.3839	9.12E-58	0.997	0.963
Epi_7	RPL37	0.4858	6.60E-55	0.981	0.88
Epi_7	RPL38	0.4692	8.73E-53	0.975	0.873
Epi_7	PDCD5	0.4247	1.18E-50	0.758	0.695
Epi_7	SHFM1	0.3857	2.60E-48	0.834	0.75
Epi_7	COX17	0.4297	4.99E-48	0.747	0.66
Epi_7	RND3	0.5611	5.24E-46	0.503	0.349
Epi_7	FAM25A	0.5336	1.54E-43	0.32	0.171
Epi_7	JUND	0.3970	1.33E-41	0.52	0.368
Epi_7	RPS21	0.3917	1.78E-40	0.918	0.814
Epi_7	RNF213	0.4501	4.32E-37	0.48	0.346
Epi_7	CDV3	0.4080	1.13E-35	0.704	0.637
Epi_7	MIDN	0.4379	3.19E-28	0.533	0.423
Epi_7	LY6D	0.5030	4.30E-28	0.691	0.576

cluster	gene	log2_avgFC	p_val_adj	pct.1	pct.2
Epi_7	JUN	0.3823	4.48E-28	0.671	0.579
Epi_7	FOSB	0.3944	3.24E-21	0.473	0.369
Epi_7	MUC1	0.3782	4.03E-20	0.413	0.315
Epi_7	MT2A	0.5162	1.35E-19	0.612	0.512
Epi_7	UPK2	0.4495	1.75E-15	0.529	0.447
Epi_7	LAMA3	0.4057	5.95E-15	0.492	0.429
Epi_7	SLC2A3	0.4928	1.17E-12	0.345	0.27
Epi_8	CD74	1.2067	0.00E+00	0.752	0.26
Epi_8	HLA-DRB1	0.8672	0.00E+00	0.527	0.119
Epi_8	HLA-DPA1	0.6175	2.85E-251	0.412	0.092
Epi_8	KRT23	1.4908	1.78E-249	0.742	0.312
Epi_8	PDZK1IP1	0.6802	6.18E-241	0.464	0.12
Epi_8	HLA-DRA	1.0005	5.28E-240	0.535	0.159
Epi_8	FXYP3	0.8534	2.27E-218	0.929	0.594
Epi_8	CRABP2	0.9997	1.14E-214	0.592	0.218
Epi_8	NAPRT	0.7518	1.10E-209	0.772	0.364
Epi_8	CST3	0.8053	6.83E-209	0.984	0.814
Epi_8	KRT20	1.0423	1.63E-198	0.921	0.64
Epi_8	KRT18	0.7239	7.11E-191	0.988	0.959
Epi_8	S100P	1.1126	1.15E-190	0.547	0.188
Epi_8	SYNGR2	0.6881	2.52E-189	0.966	0.727
Epi_8	C15orf48	0.9388	5.04E-186	0.825	0.414
Epi_8	KRT19	0.6256	9.91E-186	0.989	0.927
Epi_8	UPK2	0.8840	8.53E-170	0.803	0.426
Epi_8	CSTB	0.9192	3.58E-167	0.993	0.898
Epi_8	IFITM1	0.6745	5.68E-164	0.628	0.257
Epi_8	IL18	0.7999	1.46E-155	0.88	0.601
Epi_8	PYGB	0.6133	4.77E-154	0.812	0.466
Epi_8	SQRDL	0.5358	6.79E-154	0.647	0.301
Epi_8	LY6D	0.9774	3.65E-152	0.89	0.561
Epi_8	MMP7	1.1269	1.59E-151	0.92	0.701
Epi_8	NNMT	1.0668	4.44E-149	0.739	0.41
Epi_8	TACSTD2	0.6724	2.00E-137	0.965	0.732
Epi_8	PHLDA3	0.6480	3.26E-137	0.79	0.466
Epi_8	GSTK1	0.6005	5.39E-137	0.878	0.584
Epi_8	GPRC5A	0.5435	1.74E-136	0.967	0.771
Epi_8	RARRES3	0.8375	4.34E-135	0.769	0.421
Epi_8	CYBA	0.5865	9.15E-129	0.95	0.695
Epi_8	GLRX	0.6093	4.48E-126	0.832	0.506
Epi_8	KLK7	0.6228	1.06E-125	0.799	0.461
Epi_8	LY6E	0.5648	1.55E-123	0.976	0.796
Epi_8	CLDN3	0.6126	1.47E-121	0.955	0.735
Epi_8	S100A14	0.6373	1.63E-115	0.942	0.706
Epi_8	KRT8	0.5499	8.80E-113	0.988	0.957
Epi_8	CTS2	0.4988	2.36E-111	0.698	0.383
Epi_8	GDF15	0.6135	1.05E-109	0.698	0.364
Epi_8	TSPAN1	0.5433	9.82E-108	0.896	0.615
Epi_8	HLA-B	0.5958	5.21E-106	0.962	0.719
Epi_8	IFI6	0.6865	4.15E-102	0.896	0.599
Epi_8	CLIC3	0.5117	1.38E-89	0.811	0.498
Epi_8	C9orf16	0.5312	1.19E-85	0.963	0.766

cluster	gene	log2_avgFC	p_val_adj	pct.1	pct.2
Epi_8	LCN2	0.5867	5.59E-74	0.949	0.759
Epi_8	CKB	0.5881	6.59E-71	0.885	0.62
Epi_8	TIMP1	0.5298	1.04E-69	0.856	0.592
Epi_8	CD24	0.5548	1.80E-66	0.888	0.671
Epi_8	EDN1	0.5620	3.47E-59	0.621	0.383
Epi_8	FTL	0.5696	2.51E-27	0.998	0.938
Epi_9	MMP3	2.8318	0.00E+00	0.764	0.123
Epi_9	TSPAN8	2.3435	0.00E+00	0.819	0.151
Epi_9	AC006262.5	1.6861	0.00E+00	0.753	0.139
Epi_9	SPINK1	2.0406	6.36E-290	0.771	0.158
Epi_9	FTH1	2.0462	2.93E-242	1	0.988
Epi_9	MMP12	0.9593	8.56E-197	0.283	0.026
Epi_9	HLA-A	1.7242	1.34E-192	1	0.803
Epi_9	HLA-B	1.8590	8.61E-185	0.984	0.73
Epi_9	B2M	1.4093	8.61E-169	1	0.909
Epi_9	HPGD	1.8103	3.03E-165	0.961	0.633
Epi_9	CEACAM6	1.1783	3.94E-164	0.413	0.069
Epi_9	PERP	1.2678	8.22E-164	0.984	0.841
Epi_9	CST3	1.7680	6.67E-161	0.993	0.821
Epi_9	HLA-C	1.5152	3.78E-145	0.961	0.72
Epi_9	RP11-297P16.4	1.3326	4.06E-144	0.703	0.236
Epi_9	C15orf48	1.7445	1.61E-141	0.887	0.432
Epi_9	YPEL3	1.1569	1.52E-140	0.692	0.229
Epi_9	TPT1	0.9989	1.64E-136	0.993	0.89
Epi_9	PPDPF	1.2976	6.04E-131	0.971	0.783
Epi_9	PDZK1IP1	1.0092	6.32E-131	0.531	0.135
Epi_9	PRSS3	1.0623	1.53E-129	0.669	0.228
Epi_9	SECTM1	1.0304	1.31E-127	0.558	0.161
Epi_9	CAMK2N1	1.5277	4.54E-126	0.9	0.572
Epi_9	FXDY3	1.4384	2.12E-124	0.923	0.61
Epi_9	NEAT1	1.2845	2.29E-120	0.971	0.686
Epi_9	CD24	1.4473	1.39E-110	0.943	0.68
Epi_9	MALAT1	0.9077	4.38E-107	1	0.9
Epi_9	FTL	0.8843	9.40E-101	0.998	0.94
Epi_9	PLAT	1.2909	6.30E-100	0.603	0.211
Epi_9	PRSS8	1.0668	5.30E-98	0.712	0.33
Epi_9	CD82	1.0289	8.73E-98	0.628	0.245
Epi_9	CDA	1.0058	6.01E-96	0.873	0.65
Epi_9	SULT2B1	0.9302	8.82E-96	0.646	0.253
Epi_9	CITED2	1.2036	3.96E-93	0.692	0.304
Epi_9	KRT16	1.2962	1.96E-90	0.628	0.246
Epi_9	FXDY5	0.8947	4.20E-88	0.927	0.722
Epi_9	LIPH	1.1674	1.61E-87	0.707	0.323
Epi_9	GABARAPL1	0.8812	1.63E-87	0.522	0.173
Epi_9	GSTK1	1.0699	1.13E-86	0.859	0.599
Epi_9	SERINC2	0.9834	3.10E-81	0.834	0.566
Epi_9	PRSS22	1.1629	2.65E-64	0.841	0.567
Epi_9	ADIRF	0.9410	5.52E-63	0.984	0.849
Epi_9	CTSD	0.9664	3.92E-57	0.912	0.723
Epi_9	IFI6	1.2831	2.46E-55	0.834	0.615

cluster	gene	log2_avgFC	p_val_adj	pct.1	pct.2
Epi_9	LCN2	1.1184	1.46E-53	0.98	0.767
Epi_9	KRT17	1.0370	3.19E-48	0.85	0.584
Epi_9	GDF15	1.3826	1.04E-46	0.644	0.381
Epi_9	KLK10	0.9241	5.41E-33	0.664	0.466
Epi_9	SPRR3	1.0420	5.41E-28	0.363	0.16
Epi_9	UPK2	0.9392	1.52E-27	0.63	0.448
Epi_10	SNHG12	2.6315	0.00E+00	0.659	0.094
Epi_10	DDIT3	2.6618	1.18E-271	0.735	0.151
Epi_10	EPB41L4A-AS1	2.1125	1.66E-190	0.713	0.21
Epi_10	SNHG15	2.4521	2.82E-185	0.832	0.354
Epi_10	RSRC2	2.1336	6.21E-170	0.832	0.352
Epi_10	TAF1D	2.5748	2.54E-168	0.878	0.523
Epi_10	TXNIP	2.2981	1.07E-164	0.599	0.15
Epi_10	CYR61	2.2149	5.92E-144	0.453	0.09
Epi_10	HIST1H4H	1.5048	1.45E-127	0.263	0.033
Epi_10	ATF3	2.2331	2.87E-125	0.642	0.224
Epi_10	GADD45B	2.7686	3.17E-124	0.783	0.419
Epi_10	SNHG8	2.4073	1.58E-122	0.735	0.357
Epi_10	RBM39	1.8177	2.81E-121	0.878	0.664
Epi_10	ZFAS1	2.7501	1.08E-119	0.849	0.702
Epi_10	BRD2	1.7365	9.68E-116	0.745	0.348
Epi_10	PPP1R15A	2.1387	7.94E-115	0.83	0.526
Epi_10	SLC3A2	2.1405	4.35E-113	0.793	0.511
Epi_10	BIRC3	2.1977	2.75E-101	0.533	0.171
Epi_10	ATF4	1.7481	6.99E-100	0.798	0.476
Epi_10	CWC25	1.4870	2.23E-98	0.625	0.24
Epi_10	C6orf48	2.1230	4.07E-93	0.745	0.467
Epi_10	TRIB3	2.0802	1.15E-88	0.547	0.202
Epi_10	ZNF830	1.5164	8.11E-86	0.467	0.143
Epi_10	HIST1H2BG	2.4298	2.92E-84	0.365	0.09
Epi_10	MYC	1.6414	4.25E-79	0.484	0.169
Epi_10	HIST1H2AC	2.0745	2.21E-77	0.487	0.172
Epi_10	LUC7L3	1.4129	3.68E-77	0.74	0.418
Epi_10	NR1D1	1.8499	4.06E-75	0.543	0.216
Epi_10	SNHG19	1.4528	7.84E-72	0.394	0.117
Epi_10	CEBPB	1.7818	8.56E-72	0.691	0.448
Epi_10	SNHG7	1.6294	8.71E-71	0.713	0.466
Epi_10	OSER1	1.5709	1.41E-69	0.584	0.271
Epi_10	UPP1	1.5143	9.65E-69	0.499	0.195
Epi_10	BTG1	1.4772	6.23E-68	0.659	0.366
Epi_10	GADD45A	2.4229	2.17E-63	0.696	0.497
Epi_10	RPL22L1	1.5085	1.18E-61	0.725	0.462
Epi_10	CTA-29F11.1	1.4387	1.54E-56	0.409	0.145
Epi_10	HIST1H1C	2.5761	3.58E-56	0.589	0.318
Epi_10	HIST3H2A	1.7935	3.89E-55	0.45	0.186
Epi_10	ODC1	1.5014	7.18E-51	0.681	0.484
Epi_10	HIST1H2BD	1.5689	8.73E-46	0.372	0.139
Epi_10	DDIT4	1.4738	6.46E-42	0.477	0.227
Epi_10	CITED2	1.8845	2.52E-41	0.555	0.308
Epi_10	HIST1H2AE	1.4278	4.06E-37	0.277	0.092

cluster	gene	log2_avgFC	p_val_adj	pct.1	pct.2
Epi_10	ARRDC3	1.6578	2.88E-34	0.314	0.121
Epi_10	PMAIP1	1.6405	6.84E-29	0.655	0.514
Epi_10	G0S2	1.8180	6.79E-22	0.555	0.43
Epi_10	KRTAP2-3	1.5666	3.39E-04	0.28	0.192
Epi_10	KRTAP3-1	2.4622	1.00E+00	0.277	0.235
Epi_10	HES1	1.5499	1.00E+00	0.516	0.64
Epi_11	TUBA1A	2.3948	0.00E+00	0.921	0.078
Epi_11	IGFBP7	2.2486	0.00E+00	0.917	0.042
Epi_11	PRSS33	2.0595	0.00E+00	0.929	0.059
Epi_11	EPHB6	2.0301	0.00E+00	0.896	0.106
Epi_11	SLC14A1	2.0111	0.00E+00	0.946	0.07
Epi_11	PRF1	1.8569	0.00E+00	0.855	0.017
Epi_11	BLVRA	1.7379	8.37E-198	0.896	0.21
Epi_11	SERPINE1	1.3931	9.60E-148	0.801	0.187
Epi_11	EMP3	1.6599	1.32E-141	0.971	0.394
Epi_11	IGFBP6	2.2625	9.15E-135	0.988	0.492
Epi_11	TPM2	1.0975	6.39E-133	0.739	0.17
Epi_11	PPIA	1.9360	1.16E-121	1	0.829
Epi_11	NPC2	1.9213	5.27E-118	0.992	0.575
Epi_11	STK17A	1.0388	1.98E-106	0.701	0.187
Epi_11	CCM2	1.1150	1.26E-104	0.846	0.295
Epi_11	NT5E	1.3800	1.48E-103	0.9	0.389
Epi_11	UPP1	0.9571	3.95E-103	0.722	0.195
Epi_11	SH3BGRL3	1.2813	6.36E-101	1	0.85
Epi_11	ANXA5	1.0826	1.44E-99	0.834	0.306
Epi_11	ATOX1	1.3561	4.10E-99	0.95	0.511
Epi_11	IFI27L2	1.0578	1.49E-95	0.83	0.308
Epi_11	TMED4	1.3434	2.05E-95	0.859	0.355
Epi_11	TGFB1	1.2851	4.82E-94	0.95	0.499
Epi_11	TIMP1	1.2644	1.72E-93	0.979	0.606
Epi_11	IFI27	1.2053	4.52E-93	1	0.861
Epi_11	CD74	1.2010	1.25E-90	0.851	0.288
Epi_11	S100A6	1.1570	3.93E-89	1	0.969
Epi_11	DUSP6	1.4211	9.19E-89	0.959	0.528
Epi_11	STMN1	1.3378	2.22E-88	0.979	0.606
Epi_11	NDUFB2	1.2295	2.05E-87	0.988	0.749
Epi_11	PPP3CA	1.0392	1.40E-82	0.693	0.208
Epi_11	LGALS1	1.3434	1.87E-82	0.996	0.75
Epi_11	NPW	1.2271	3.77E-81	0.971	0.524
Epi_11	PSMA2	1.2667	1.59E-79	0.9	0.506
Epi_11	MET	1.1755	1.81E-78	0.959	0.604
Epi_11	PTMS	0.9962	7.60E-74	0.992	0.696
Epi_11	PLK2	1.0595	9.37E-74	0.867	0.384
Epi_11	POLD2	1.1827	1.87E-73	0.905	0.468
Epi_11	RPL22L1	1.2351	4.67E-70	0.876	0.463
Epi_11	TES	0.9738	4.16E-69	0.851	0.39
Epi_11	ANKRD1	1.0353	1.41E-67	0.419	0.09
Epi_11	MT-ND3	1.1342	4.41E-66	1	0.747
Epi_11	H2AFV	1.4779	1.16E-57	0.863	0.518
Epi_11	AREG	1.1939	7.51E-56	0.975	0.7
Epi_11	ISG15	1.0550	2.41E-54	0.988	0.727

cluster	gene	log2_avgFC	p_val_adj	pct.1	pct.2
Epi_11	RHOBTB3	1.0621	1.73E-50	0.801	0.41
Epi_11	MDK	1.0745	1.98E-46	0.805	0.417
Epi_11	CAV1	1.1569	1.36E-44	0.983	0.712
Epi_11	IGFBP1	1.2287	2.93E-44	0.606	0.241
Epi_11	CAV2	0.9671	1.57E-39	0.921	0.648